

Fermi National Accelerator Laboratory

FN-498

**Coherent Instability Limitations
of pp and $\bar{p}p$ Upgrade Scenarios**

S. A. Bogacz
Accelerator Theory Department
Fermi National Accelerator Laboratory
P.O. Box 500, Batavia, Illinois 60510

October 1988



Operated by Universities Research Association Inc. under contract with the United States Department of Energy

COHERENT INSTABILITY LIMITATIONS OF pp AND $p\bar{p}$ UPGRADE SCENARIOS

S.A. Bogacz

Accelerator Theory Department, Fermi National Accelerator Laboratory*,

P.O. Box 500, Batavia, IL 60510, USA

October 1988

ABSTRACT

A survey of various intensity limitations due to the coherent instabilities is carried out in the context of forecoming upgrades of both fixed target and collider operational modes. A comprehensive study of the transverse and longitudinal coupling impedance of the Tevatron is further extended to estimate the impedance of the Main Ring and the proposed Main Injector. The result is summarized in terms of the effective impedances constructed for particular longitudinal and transverse beam spectra corresponding to specific instabilities. A number of potentially offending instabilities were tentatively selected for further study. They are discussed in two separate categories: single bunch instabilities, e.g. fast microwave instability (longitudinal and transverse), colliding mode instability (longitudinal and transverse), slow head-tail instability (transverse) and multi-bunch instabilities: e.g. coupled bunch instability driven by the resistive wall impedance (transverse). Further detailed analysis of the above instabilities for proposed upgrade scenarios reveal specific constraints and limitations, which they put on various beam parameters.

* Operated by the Universities Research Association under contract with the U.S. Department of Energy

INTRODUCTION

This study is motivated by the proposed upgrades of a whole sequence of Fermilab's accelerators; Linac, Booster, Main Ring or Main Injector and the Tevatron. Two leading high-luminosity collider upgrade scenarios, pp and $p\bar{p}$, involve larger numbers of colliding bunches of higher intensity and smaller transverse emittance. Other parameters like betatron tunes and longitudinal phase-space characteristics are also altered. This obviously raises a question of coherent instabilities, which was already quite vital in the present fixed target and collider scenarios. One might be concerned that the new demanding list of parameters may push coherent instabilities beyond the curable region, where presently used suppressing schemes like active dampers and various Landau damping cures are no longer feasible. To clarify and answer some of these questions on a more quantitative ground, a number of possibly offending single bunch instabilities were examined for both collider and fixed target operational modes. Furthermore, multi-bunch instability limitations due to the resistive wall impedance are also studied for the fixed target mode. The same question of coupled bunch instabilities is also addressed for new collider schemes involving large number of colliding bunches (up to 100 on 100 bunches), where the inter-bunch communication may become important. Each of the above instabilities results in a specific constraint defining a stable region in the intensity-tune-emittance parameter space. Individual regions are combined together into the net constraint. A brief discussion of the stability regions for various operational modes is included in the closing part of each section of this study. An overall summary of the coherent instability limitations of the proposed upgrades is presented in the last section of this study (see Sec.6).

1. COUPLING IMPEDANCES

Here we present a systematic study of the longitudinal and transverse coupling impedance of the Tevatron. Some of these results will be further extended to estimate the impedance of the Main Ring and the Main Injector.

We tentatively identified four dominant sources of the Tevatron's coupling impedance. These potentially offending vacuum structures are listed as follows:

- (a) bellows
- (b) kicker magnets
- (c) beam position monitors
- (d) resistive wall and Lambertson magnet laminations.

One can estimate both longitudinal and transverse impedances induced by the above elements, using simple quantitative models discussed in detail below:

(a) The first contribution was simulated numerically using the TBCI code¹ (real time solution of the Maxwell equations for a given geometry excited by a Gaussian test bunch). Calculated fast Fourier transforms of both the longitudinal and the transverse wake fields are translated into the longitudinal and transverse impedances respectively. The results are illustrated in Fig.1. Assuming low- Q resonance character of the above solutions each of the broad-band resonances can be parametrized by the shunt impedance R , the quality factor Q and the resonant frequency ω . The resulting fit for the longitudinal impedance is summarized by

$$Z_{\parallel}(\omega) = \frac{R_s}{1 + iQ_{\parallel}(\omega/\omega_{\parallel} - \omega_{\parallel}/\omega)} \quad (1.1)$$

where

$$R_s = 1.3 \times 10^5 \text{ Ohm}$$

$$Q_{\parallel} = 2.3$$

$$\omega_{\parallel} = 2\pi \times 8 \text{ GHz,}$$

and it is illustrated graphically in Fig.2a.

Similarly the transverse impedance fit is expressed as follows

$$Z_{\perp}(\omega) = \frac{R_t \omega/\omega_{\perp}}{1 + iQ_{\perp}(\omega/\omega_{\perp} - \omega_{\perp}/\omega)} , \quad (1.2)$$

where

$$R_t = 1.2 \times 10^6 \text{ Ohm/m}$$

$$Q_{\perp} = 3.4$$

$$\omega_{\perp} = 2\pi \times 8 \text{ GHz.}$$

The above contribution is plotted in Fig.3a.

(b) There are eleven kicker magnets; both injection and abort kickers located around the ring. According to Ref.2 the real and imaginary part of the longitudinal coupling impedance of a c-magnet of the characteristic impedance Z_s and length L are given by the following analytic expressions

$$\text{Re } Z_{\parallel}(\omega) = \frac{Z_s}{2} \cos^2 \frac{\omega L}{c} , \quad (1.3)$$

$$\text{Im } Z_{\parallel}(\omega) = \frac{Z_s}{2} \left\{ \frac{\omega L}{c} - \sin \frac{\omega L}{c} \right\} , \quad (1.4)$$

where

$$Z_s = 6 \text{ Ohm}$$

$$L = 1 \text{ m}$$

Similarly, the real and imaginary parts of the transverse coupling impedance of a c-magnet of half-width a , half-height b and length L are expressed as follows

$$\text{Re } Z_{\perp}(\omega) = \frac{Z_0 c}{4ab} \frac{1}{\omega} \left\{ 1 - \cos \frac{\omega L}{c} \right\} , \quad (1.5)$$

$$\text{Im } Z_{\perp}(\omega) = \frac{Z_0 c}{4ab} \frac{1}{\omega} \left\{ \frac{c}{\omega L} - \sin \frac{\omega L}{c} \right\} , \quad (1.6)$$

where

$$Z_0 = 377 \text{ Ohm}$$

$$L = 1 \text{ m}$$

$$a = 3.7 \text{ cm}$$

$$b = 1.9 \text{ cm.}$$

Both contribution to coupling impedances given by Eqs.(1.3)–(1.4) and Eqs.(1.5)–(1.6) are illustrated in Figs. 2b and 3b respectively.

(c) Similar contribution comes from 108 beam position monitors. Each unit consists of a pair of cylindrical strips of length l and width $b\phi_0$ forming a simple transmission line of the characteristic impedance Z_s . The longitudinal coupling impedance is expressed as follows²

$$Z_{\parallel}(\omega) = Z_s \left\{ \frac{\phi_0}{2\pi} \right\}^2 \times \left\{ \sin^2 \frac{\omega l}{c} - i \sin \frac{\omega l}{c} \cos \frac{\omega l}{c} \right\}, \quad (1.7)$$

where

$$l = 18 \text{ cm}$$

$$Z_s = 50 \text{ Ohm}$$

$$b = 3.5 \text{ cm}$$

$$\phi_0 = 1.92 \text{ rad.}$$

The transverse impedance is expressed in terms of the above longitudinal impedance according to the following relationship

$$Z_{\perp}(\omega) = c \left\{ \frac{4}{b\phi_0} \right\}^2 \times \sin^2 \frac{\phi_0}{2} \times \frac{Z_{\parallel}(\omega)}{\omega} , \quad (1.8)$$

A graphical illustration of Eqs.(1.3)–(1.4) is given in Figs. 2c and 3c.

(d) Finally, the low frequency contribution to the longitudinal impedance due to the resistive wall and Lambertson magnet laminations is given by the following standard expression³

$$Z_{\parallel}(\omega) = (1 - i) \frac{R}{\delta \sigma b} , \quad (1.9)$$

where the skin depth, δ , is defined as follows

$$\delta = \sqrt{\frac{2}{\mu_0 \sigma \omega}} \quad (1.10)$$

Here $\sigma = 2 \times 10^6 \text{ Ohm}^{-1} \text{ m}^{-1}$ is the resistivity of the stainless steel, $\mu_0 = 4\pi \times 10^{-7} \text{ N A}^{-2}$ is the free space permeability and $b = 3.49 \text{ cm}$ is the vacuum pipe radius. The transverse and longitudinal resistive wall impedances are connected through the following well known relationship

$$Z_{\perp}(\omega) = \frac{2c}{\omega b^2} \times \frac{Z_{\parallel}(\omega)}{\omega} , \quad (1.11)$$

Similarly, formulas given by Eqs.(1.9) and (1.11) are illustrated in Figs.2d and 3d.

We notice in passing that for very small frequencies the skin depth, δ , becomes larger than the vacuum pipe thickness, Δ , therefore the electromagnetic fields induced by the **ac** component of the beam current penetrate the beam pipe and leak outside it. Below the cross-over region ($\delta \sim \Delta$), at sufficiently lower frequencies, one can assume that the vacuum pipe wall is completely penetrated by the ac fields induced by the beam current. This argument justifies why in the low frequency regime, Δ , replaces, δ , in the above formulas, Eqs.(1.9) and (1.11).

All four contributions to both the longitudinal and transverse impedance are summarized by the net impedances illustrated in Fig.4. One can notice (see Fig.2a) that the longitudinal impedance is virtually dominated by the broad-band contribution (bellows). Similarly, bellows contribute substantially to the broad-band part of the transverse impedance (see Fig.3a), together with the kicker magnets, which significantly raise the reactive component of the impedance spectrum (see Fig.3b). Finally, the low frequency region of the transverse impedance is dominated by the singular resistive wall contribution (see Fig.3d).

The above summary of coupling impedances will serve as a starting point for the calculation of the effective impedance, which will be carried out in a few consecutive sections.

2. MICROWAVE INSTABILITY

The classical picture of the microwave instability⁴ assumes that the wavelength of the perturbing field is much shorter than the bunch length. In a limit of fast blow-up (the characteristic growth-time much shorter than the synchrotron period) one can use a modified Boussard criterion to define the instability threshold. These threshold conditions for both the longitudinal and transverse instabilities are summarized as follows⁴

$$|Z_{\parallel}/n| \leq \frac{2\pi |\eta| (E/e) \delta_p^2}{I_p} \quad (2.1)$$

and

$$|Z_{\perp}| \leq \frac{4 \sqrt{2\pi} |\eta| (E/e) n \delta_p}{I_p \langle \beta \rangle} \quad (2.2)$$

where $\langle \beta \rangle$ denotes the average beta-function, η is the frequency dispersion parameter and n is the harmonic number corresponding to the peak of the broad-band impedance, or is equal to the cut-off harmonic, $n \approx R/2b$, in case of the space charge impedance. Furthermore, $\delta_p \equiv \sigma_p/p$, represents the fractional rms longitudinal momentum spread and I_p is the peak current of a bunch containing N particles. Both quantities are given explicitly as follows

$$I_p = \frac{eNc}{\sqrt{2\pi} \sigma_l} \quad (2.3)$$

and

$$\delta_p = \sqrt{\frac{e \hat{V}}{\pi h |\eta| E} \left(1 - \cos \frac{h \sigma_l}{R} \right)} \quad (2.4)$$

where \hat{V} denotes the rf voltage amplitude, σ_l is the rms bunch-length, E is the total energy of a proton and R is the radius of the ring. The last formula⁵, Eq.(2.4), is valid for a stationary bucket, therefore a storage ring mode (no acceleration) is assumed.

The above condition combined with Eqs.(2.1) and (2.2) yields the following intensity thresholds for the microwave instability

$$N_{\parallel} = \frac{(\sqrt{2\pi})^3 \sigma_f(E/e) |\eta| \delta_p^2}{e c |Z_{\parallel}/n|} \quad (2.5)$$

and

$$N_{\perp} = \frac{8\pi \sigma_f(E/e) |\eta| n \delta_p}{e c \langle \beta \rangle |Z_{\perp}|} \quad (2.6)$$

Here N_{\parallel} and N_{\perp} denote critical bunch intensities corresponding to the longitudinal and transverse microwave instabilities respectively.

A finite-size beam, modelled by a cylinder of radius a , interacting with a conducting vacuum pipe of radius b , is a subject to coherent space-charge force both in the longitudinal and the transverse directions (if the beam is slightly displaced off-axis). The space-charge induced wake fields are conveniently expressed in terms of the coupling impedances according to the following formulas²

$$|Z_{\parallel}/n| = \frac{Z_0}{2\beta\gamma^2} \left\{ 1 + 2 \ln \frac{b}{a} \right\} \quad (2.7)$$

and

$$|Z_{\perp}| = \frac{RZ_0}{2\beta^2\gamma^2} \left\{ \frac{1}{a^2} - \frac{1}{b^2} \right\} \quad (2.8)$$

where $Z_0 = 377$ Ohm is the free space impedance and γ is the Lorentz contraction factor. The transverse beam size parameter, a , is defined in terms of the transverse emittance, ϵ , as follows

$$a = \sqrt{\frac{\epsilon \langle \beta \rangle}{\pi}} \quad (2.9)$$

Other significant contributions to the effective impedances $|Z_{||}/n|$ and $|Z_{\perp}|$ come from the broad-band part illustrated in Figs.2a and 3a. According to the generic spectral averaging procedure⁴ the effective impedances are defined as follows

$$|Z_{||}/n| = \int_{-\infty}^{\infty} d\omega \rho_0(\omega) \frac{Z_{||}(n\omega_0 + \omega)}{\omega/\omega_0} , \quad (2.10)$$

$$|Z_{\perp}| = \int_{-\infty}^{\infty} d\omega \rho_0(\omega) Z_{\perp}(n\omega_0 + \omega) \quad (2.11)$$

and

$$\rho_0(\omega) = \frac{\sigma_L}{\sqrt{\pi} c} \exp\left(-\frac{(\omega \sigma_L)^2}{c^2}\right) , \quad (2.12)$$

where ρ_0 is the unperturbed longitudinal spectrum of the bunch normalized to unity. If the width of the beam spectrum is much smaller than the widths of the broad-band resonances ($c/\sigma_L \ll Q_{||} \omega_{||}$ and $Q_{\perp} \omega_{\perp}$) one can assume that both impedances are frequency independent and can be taken outside the integration in the above formulas. This assumption is perfectly valid for broad-band impedances considered here (see Fig.4) as long as the bunches are not extremely short ($\sigma_L \sim 10^{-3}$ m). Frequency dependence of $|Z_{||}|/n$ is illustrated in Fig.5; its maximum is taken as the value of $|Z_{||}/n|$. The numerical values of both $|Z_{||}/n|$ and $|Z_{\perp}|$, taken at harmonic n , are listed as follows

$$|Z_{||}/n| = 0.83 \text{ Ohm}$$

and

$$|Z_{\perp}| = 2.3 \times 10^6 \text{ Ohm m}^{-1}$$

where

$$n = 1.5 \times 10^5.$$

Substituting Eqs.(2.5)–(2.9) into the threshold conditions given by Eqs.(2.1)–(2.2) one can calculate both longitudinal and transverse critical bunch intensities (N_{sc}) as a function of the transverse emittance. Similarly, applying the impedance formulas, expressed by Eqs.(2.10)–(2.12), to the general microwave threshold conditions given by Eqs.(2.1)–(2.2) one can calculate the broad-band contributions to the instability threshold (N_{b-b}). Finally, combining both constrains one can express the overall critical intensity according to the obvious formula

$$\frac{1}{N} = \frac{1}{N_{sc}} + \frac{1}{N_{b-b}} \quad (2.13)$$

All three curves calculated for various operational modes of the Tevatron, Main Ring and Main Injector, for both the longitudinal and transverse intensity thresholds are illustrated in Figs. 6–10. One can see from Fig.6 and 7, that in case of the Tevatron and new Tevatron, for typical beam emittances ($\epsilon \geq 6\pi$ mm mrad) the broad-band contribution to the instability is dominant and it sets the microwave instability thresholds. As can be seen from Table 1, the Tevatron's thresholds are not very restrictive (especially the transverse one), therefore one should not expect any danger of the microwave instability; even for very short bunches ($\sigma_z \sim 10^{-1}$ m) and small transverse emittances ($\epsilon \sim 1$ mm mrad) as long as the bunch intensities do not significantly exceed 10^{11} ppb. The weak dependence of these thresholds on the transverse beam size, suggests marginal influence of the coherent space charge wake fields on the microwave instability. Nevertheless, its real counterpart (Laslett betatron tune shift) may prove to be the dominant effect of the space charge on the coherent motion of the beam.

As one might expect in the lower energy range (the Main Ring, Main Injector) the microwave instability is space-charge dominated. This feature is explicitly visible in Figs.8 and 10 representing the microwave instability thresholds at injection to the Main

Ring and Main Injector and in Figs.9 and 11, which describe proton storage just above the transition in both machines. In principle, (see Eq.2.5 and 2.6) exactly at transition, a beam is always unstable against the microwave instability, however as illustrated in Figs. 9 and 10, the beam quickly gains stability shortly after transition. Characteristic threshold values collected in Table 1 show slightly lower thresholds for the Main Ring compared to the Main Injector, nevertheless both machines test quite well against the microwave instability, for the considered upgrade scenarios (see Table 1).

$$\varepsilon = 6\pi \text{ mm mrad}$$

σ_t [m]	$\langle\beta\rangle$ [m]	h	R [m]	E [GeV]	N_{\parallel} [ppb]	N_{\perp} [ppb]
Tevatron (p-injection)						
0.1	56.7	1113	1×10^3	150	1.6×10^{11}	1.7×10^{13}
0.3	56.7	1113	1×10^3	150	4.2×10^{12}	1.5×10^{14}
Main Ring (p-injection)						
0.1	56.7	1113	1×10^3	8.9	2.4×10^{10}	5.3×10^{10}
0.3	56.7	1113	1×10^3	8.9	6.4×10^{11}	4.7×10^{11}
Main Ring (p-storage)						
0.1	56.7	1113	1×10^3	25	9.3×10^{10}	2.3×10^{11}
0.3	56.7	1113	1×10^3	25	2.5×10^{12}	2.1×10^{12}
Main Injector (p-injection)						
0.1	30	578	519.4	8.9	3.2×10^{10}	5.8×10^{10}
0.3	30	578	519.4	8.9	8.6×10^{11}	5.2×10^{11}
Main Injector (p-storage)						
0.1	30	578	519.4	25	1.4×10^{11}	2.6×10^{11}
0.3	30	578	519.4	25	3.7×10^{12}	2.3×10^{12}

Table 1

3. MODE COLLIDING INSTABILITY

Moving to the lower part of the frequency spectrum one encounters the so called mode colliding instability. The characteristic wavelength of the instability is of the order of the bunch length and its growth time is somewhat longer than the synchrotron period. At small currents coherent motion (both longitudinal and transverse) of a single bunch (in the moving reference frame) can be described in terms of its multipole modes; $m = 1$ (dipole), $m = 2$ (quadrupole) etc. at frequencies separated by $m\omega_0 v_s$, respectively. However, these frequencies are intensity dependent due to the self-induced wake fields. As the current increases, the coherent frequencies of these modes move and at some point two modes may cross. The resulting degeneracy of two eigensolutions is responsible for the colliding mode instability. As we mentioned before, it has both longitudinal and transverse realizations. Its transverse version is better known as the strong head-tail instability. If the bunches are not too long ($\sigma_l \sim 1$ m), the strongest coherent tune shift occurs for the rigid motion of the bunch (dipole mode) and this mode will more likely cross first (with the lower branch of the quadrupole mode, $m = -1$). Assuming a Gaussian bunch the coherent tune shift for $m = 0$ mode (longitudinal and transverse) are given by the following expressions

$$\Delta v_{\parallel} = - \frac{i \eta I_p}{4 (\sqrt{2\pi})^3 (E/e) v_s} \left(\frac{R}{\sigma_l} \right)^2 \langle Z_{\parallel}/n \rangle \quad (3.1)$$

and

$$\Delta v_{\perp} = - \frac{i \langle \beta \rangle I_p}{4\pi \sqrt{2} (E/e)} \langle Z_{\perp} \rangle . \quad (3.2)$$

Here I_p is the peak current previously given by Eq.(2.3) and the effective impedance is defined in terms of the following spectral averages $\langle \dots \rangle$

$$\langle Z_{\parallel}/n \rangle = \int_{-\infty}^{\infty} d\omega \rho_0(\omega) \frac{Z_{\parallel}(\omega)}{\omega/\omega_0} \quad (3.3)$$

and

$$\langle Z_{\perp} \rangle = \int_{-\infty}^{\infty} d\omega \rho_0(\omega) Z_{\perp}(\omega) \quad , \quad (3.4)$$

with the longitudinal bunch spectrum, $\rho_0(\omega)$, given by Eq.(2.10). Since the adjacent modes are separated by the synchrotron frequency, $\omega_s = v_s \omega_0$, an approximate mode crossing condition can be written in a generic form as

$$\text{Re} \frac{\Delta v}{v_s} \approx 1 \quad (3.5)$$

where the synchrotron tune for an elliptic bunch in a stationary bucket is given by the following formula

$$v_s = \sqrt{\frac{e \hat{V} h |\eta|}{2\pi E}} \quad . \quad (3.6)$$

The above condition combined with Eqs.(3.1) and (3.2) yields the following intensity thresholds for the colliding mode instability

$$N_{\parallel} = \frac{(4\pi)^2 \sigma_f (E/e) v_s^2}{e c |\eta| \text{Im} \langle Z_{\parallel}/n \rangle} \left(\frac{\sigma_f}{\bar{R}} \right)^2 \quad (3.7)$$

$$N_{\perp} = \frac{8(\sqrt{\pi})^3 (E/e) \sigma_f v_s}{e c \langle \beta \rangle \text{Im} \langle Z_{\perp} \rangle} \quad (3.8)$$

Here N_{\parallel} and N_{\perp} denote critical bunch intensities corresponding to the longitudinal and transverse colliding mode instabilities respectively. One can notice in passing, that the above pair of threshold conditions is somehow similar to the thresholds for the microwave instabilities. The crucial difference lies in the effective impedance definition, Eqs.(3.3)–(3.4). Here the beam spectrum samples the low frequency region of the coupling impedances, contrary to the microwave instability driven by the higher frequency contributions (near the cut-off frequency). Therefore, in case of the colliding mode instability, there are two dominant contributions to the effective impedances: the broad-band contribution and the resistive wall impedance. Again, the broad-band impedance (at $\omega = 0$) is almost flat on a scale of the spectral width of a typical bunch and can be safely taken outside the integration in Eqs.(3.3) and (3.4). On the other hand, in case of the resistive wall impedances, given by Eqs.(1.9)–(1.11), these integrals will involve singular integrands (at $\omega = 0$). However, explicitly carried out integration removes the singularity and yields a finite result. Both contributions to the effective impedance, together with their numerical values, are summarized in Table 2.

Contribution	$\text{Im} \langle Z_{\parallel}/n \rangle$ [Ohm]	$\text{Im} \langle Z_{\perp} \rangle$ [Ohm/m]
broad-band	$\frac{R_s \omega_0}{Q_{\parallel} \omega_{\parallel}}$	$\frac{R_t}{Q_{\perp}}$
resistive wall	$\Gamma\left(\frac{1}{4}\right) \sqrt{\frac{\mu c \sigma_f}{2\pi\sigma}} \frac{1}{b}$	$\Gamma\left(\frac{1}{4}\right) \sqrt{\frac{\mu c \sigma_f}{2\pi\sigma}} \frac{2R}{b^3}$
Tevatron		
broad-band	0.34	0.35×10^6
resistive wall	$0.57 \sqrt{\sigma_f}$	$0.94 \times 10^6 \sqrt{\sigma_f}$
Main Ring		
broad-band	0	0
resistive wall	$0.57 \sqrt{\sigma_f}$	$0.94 \times 10^6 \sqrt{\sigma_f}$
Main Injector		
broad-band	0	0
resistive wall	$0.57 \sqrt{\sigma_f}$	$0.49 \times 10^6 \sqrt{\sigma_f}$

Table 2

The critical bunch intensities calculated according to formulas given by Eqs.(3.7) and (3.8) for various operational modes of the Tevatron, Main Ring and Main Injector are illustrated in Figs.12–14. A summary of the colliding mode instability thresholds is included in Table 3. As one can see from Table 3 the transverse threshold is always about two orders of magnitude lower than the longitudinal one, and still the transverse colliding mode instability is safe below intensities of 10^{12} ppb. Figures 12–14 show that the instability thresholds weakly depend on energy and the transition crossing for all cases considered here.

σ_r [m]	$\langle\beta\rangle$ [m]	h	R [m]	E [GeV]	N_{\parallel} [ppb]	N_{\perp} [ppb]
Tevatron (p-injection)						
0.1	56.7	1113	1×10^3	150	2.6×10^{12}	9.5×10^{11}
0.3	56.7	1113	1×10^3	150	5.6×10^{13}	2.1×10^{12}
Main Ring (p-injection)						
0.1	56.7	1113	1×10^3	8.9	7.4×10^{12}	9.7×10^{11}
0.3	56.7	1113	1×10^3	8.9	1.2×10^{14}	1.7×10^{12}
Main Ring (p-storage)						
0.1	56.7	1113	1×10^3	25	7.4×10^{12}	5.5×10^{11}
0.3	56.7	1113	1×10^3	25	1.2×10^{14}	9.6×10^{11}
Main Injector (p-injection)						
0.1	30	578	519.4	8.9	1.6×10^{13}	2.4×10^{12}
0.3	30	578	519.4	8.9	1.9×10^{14}	4.2×10^{12}
Main Injector (p-storage)						
0.1	30	578	519.4	25	1.3×10^{13}	1.4×10^{12}
0.3	30	578	519.4	25	1.9×10^{14}	2.4×10^{12}

Table 3

4. RESISTIVE WALL COUPLED-BUNCH INSTABILITY

Assuming M equally spaced bunches in a storage ring environment, characterized by the transverse coupling impedance, Z_{\perp} , there are in principle M possible dipole modes of coherent transverse motion of the ensemble of M rigid bunches. Each mode, labeled by $m = 1, \dots, M$, is described by its characteristic growth-time, τ_m , given by the following formula

$$\frac{1}{\tau_m} = - \frac{e c M I_b}{4\pi v_{\beta} E} \sum_{p=-\infty}^{\infty} \text{Re } Z_{\perp}((pM - m + v_{\beta}) \omega_0) \quad (4.1)$$

where I_b is the average current of one bunch and v_{β} is the betatron tune. The above notation assumes that the negative values of τ_m correspond to the stable modes (damping). Coupling of adjacent bunches requires relatively long-range wake fields; long enough to span the gap between neighboring bunches. In the frequency domain this long-range wake field contributions may be provided either by the high- Q parasitic resonances of the rf cavities, or by the resistive wall zero-frequency singularity. The first contribution is rarely present (its longitudinal equivalent is usually more pronounced), therefore we will ignore it in our discussion and confine our consideration to the low frequency resistive wall impedance only. Substituting explicit expression for Z_{\perp} , Eqs.(1.9)–(1.11), into Eq.(4.1) reduces the infinite summation over the sampling frequencies to a single dominant line only (the closest sampling frequency is $\pm M\omega_0$ away from the dominant line and the singular impedance drops to a negligibly small value). Since the singularity appears at $\omega = 0$ the dominant line is fixed by the minimum of the following expression

$$| pM - m + v_{\beta} | \quad (4.2)$$

A simple numerology shows that the above condition is satisfied if $p = 0$ and $m = \text{Int}(v_\beta) + 1$ (the coupled-bunch mode index is equal to the closest upper integer of the betatron tune). Now the effective impedance in Eq.(4.1) is approximately given by

$$\sum_{p=-\infty}^{\infty} Z_{\perp}((pM - m + v_\beta) \omega_0) \rightarrow Z_{\perp}((v'_\beta - 1) \omega_0) \quad (4.3)$$

where the fractional tune is defined as follows

$$v'_\beta = v_\beta - \text{Int}(v_\beta) \quad (4.4)$$

Here Int denotes the integer part of a real number.

One has to be cautious to maintain the proper analytic behavior of $Z_{\perp}(\omega)$ in the low frequency region. As was mentioned in Sec.2, the skin depth, δ , corresponding to the dominant line frequency, $(v'_\beta - 1) \omega_0$, should be compared with the vacuum pipe thickness, Δ . If the betatron tune is below half-integer then $\delta \ll \Delta$ and one can use the analytic expression for $Z_{\perp}(\omega)$ given by Eqs.(1.9)–(1.11). The other extreme regime is present if the tune is very close to the upper integer, then the inequality reverses, $\Delta \ll \delta$, and one has to make the following substitution in Eq.(1.9): $\delta \rightarrow \Delta$. Keeping in mind the above remark one can use Eqs.(4.1) and (4.3) to evaluate the characteristic growth-times, τ_m , of the dominant modes for various storage ring conditions corresponding to considered Tevatron – Main Ring (Main Injector) upgrades.

The quantitative results are summarized in Table 4 and further illustrated in Figs. 15–17. One can see that for the high intensity fixed target scenario ($N_b = 5 \times 10^{10}$) the injection to the Tevatron is limited by the transverse instability with the characteristic growth-time of about 30 msec., which can easily be suppressed by a feedback system. On the other hand, the same high intensity injection to the Main Ring

faces very fast transverse instability with the order of magnitude shorter growth-time than the Tevatron's; this may pose a serious problem for an active damper and one may have to resort to a strong Landau damping decoherence scheme eg. octupole tune spread, which is able to suppress the instability. The Main Injector design seems to be quite resistant to the transverse coupled bunch instability; even for high intensity injection the characteristic growth-time is about 12 msec. which may be handled by a fast feedback system. For the new collider mode with 96 on 96 high intensity bunches ($N_b = 5 \times 10^{10}$) the communication between bunches is quite significant and it yields to the growth-time of about 300 msec., which may call for a damper system for the collider mode as well.

ν_β	m	M	N_b [ppb]	E [GeV]	τ_m [sec]
Tevatron (collider)					
20.415	21	53	6×10^{10}	150	5.59×10^{-1}
20.415	21	96	6×10^{10}	150	3.09×10^{-1}
Tevatron (fixed target)					
19.456	20	1008	2×10^{10}	150	8.11×10^{-2}
19.456	20	1008	5×10^{10}	150	3.24×10^{-2}
New Tevatron (fixed target)					
20.6	21	996	2×10^{10}	150	7.36×10^{-2}
20.6	21	996	5×10^{10}	150	2.94×10^{-2}
Main Ring (p-storage)					
19.4	20	1008	2×10^{10}	8.9	5.04×10^{-3}
19.4	20	1008	5×10^{10}	8.9	2.01×10^{-3}
Main Injector (p-storage)					
22.4	23	498	2×10^{10}	8.9	1.63×10^{-2}
22.6	23	498	5×10^{10}	8.9	1.35×10^{-2}

Table 4

5. SLOW HEAD-TAIL INSTABILITY

Finally, one should examine a high frequency (500 – 900 MHz region), single-bunch transverse instability, known as the slow head-tail instability. First, we will start with a brief discussion of the experimental evidence and characteristic signature of this instability, then our study will be extended to the prospective upgrade scenarios.

The instability was first observed⁶, in combination with the low frequency resistive wall component, during the recent 1987–88 Tevatron fixed target run. In the present operating mode 1000 consecutive bunches are loaded into the machine at 150 GeV with a bunch spacing of 18.8×10^{-9} sec. (53 MHz). The normalized transverse emittance is typically $15 \pi \times 10^{-6}$ m rad in each plane with a longitudinal emittance of about 1.5 eV-sec. The beam is accelerated to 800 GeV in 13 sec. and then it is resonantly extracted during a 23 sec. 'flat top'. As the run progressed the bunch intensities were increased until at about 1.4×10^{10} ppb the beam experienced the onset of a coherent horizontal oscillation taking place in the later stages of the acceleration cycle (> 600 GeV). This rapidly developing coherent instability results in a significant emittance growth, which limits machine performance and in a catastrophic scenario it even prevents extraction of the beam.

The characteristic feature of the instability is that it was only observed in the horizontal plane and the oscillation was self-stabilizing at the 2–3 mm betatron amplitude level. The effect was non-resonant, with no strong dependence on the tune. Furthermore, the instability growth-time could be increased by reducing the chromaticity to be positive but close to zero (1–2 units). However, the most successful method of suppressing the instability was achieved by increasing the longitudinal emittance via white noise applied to the rf drive; an emittance of 5 eV-sec. would permit a bunch intensity of about 1.8×10^{10} ppb. The growth time was fast; less than 30×10^{-3} sec. Typically, the full ring would go unstable, but we have observed⁶ unstable behavior

in a partial azimuth of the ring when bunches of significantly higher intensity were present.

As was shown in Ref. 6, through a systematic numerical analysis of the Sacherer's model⁷, the resulting growth-time vs chromaticity plots suggest existence of the $l \geq 1$ slow head-tail modes as a plausible mechanism for the observed coherent betatron instability. This last claim is based on a very good agreement between the measured values of the instability growth-time and the ones calculated on the basis of presented model.⁶

One obviously expects, that even more pronounced version of this instability will also be present in the proposed high-intensity upgrades. Therefore, we should examine its prospective strength in the Tevatron, Main Ring and the Main Injector. Encouraged by the successful explanation of the Tevatron's instability⁶ we will apply the same intuitive model of the slow head-tail instability to examine the impact of this instability on various upgrade scenarios involving the Tevatron, Main Ring and Main Injector.

Following the Sacherer's model⁷ one assumes that the amplitude of the transverse beam oscillation (related to the pick-up monitor signal) is a superposition of a standing plane wave pattern (with the number of internal nodes defining the longitudinal mode index l) and a propagating part describing the betatron phase lag/gain, governed by the characteristic chromatic frequency, $\omega_\xi = \xi\omega_0/\eta$. One can easily find the power spectrum of the transverse beam signal by taking the Fourier transform of the amplitude signal. The resulting beam spectrum is shifted by ω_ξ due to the presence of the propagating wave component (finite chromaticity). Periodicity given by the revolution period, $2\pi/\omega_0$, yields the discrete frequency spectrum with spacing ω_0 .

$$\omega_p = (p + \nu)\omega_0 , \quad (5.1)$$

where p is an integer. The explicit form of the power spectrum is given by the following expression⁷

$$\rho^{(\ell)}(\omega) = \frac{h^{(\ell)}(\omega)}{\sum_{p=-\infty}^{\infty} h^{(\ell)}(\omega_p)} \quad .$$

where

(5.2)

$$h^{(\ell)}(\omega) = \frac{4}{\pi^2} (\ell + 1) \frac{1 + (-1)^\ell \cos(2\omega\hat{\tau})}{[(2\omega\hat{\tau}/\pi)^2 - (\ell + 1)^2]^2} \quad .$$

which will serve as a spectral density function in evaluation of the averaged transverse coupling impedance. Assuming small amplitude (harmonic) synchrotron motion, $\hat{\tau}$ is given by the following expression

$$\hat{\tau} = \sqrt[4]{\frac{2\varepsilon^2\eta}{\pi\omega_0^2 E_0 \gamma e V \cos\phi_s}} \quad . \quad (5.3)$$

Here ε is the longitudinal emittance (eV-sec), E_0 is the rest energy of a proton, \hat{V} is the amplitude of the rf voltage, ϕ_s is the synchronous phase and γ is the Lorentz contraction factor.

Following Sacherer's argument⁸, one can generalize a simple equation of motion describing a wake field driven coherent betatron motion of a coasting beam to model the head-tail instability of the bunched beam. A simple dipole oscillation of the individual Fourier components of the beam is governed by the following equation⁸

$$(v\omega_0)^2 - \Omega_c^2 - i \frac{e\beta}{\gamma m_0} \frac{I_0}{2\hat{\tau}c} \frac{1}{\ell + 1} \sum_{p'=-\infty}^{\infty} Z_{\perp}(\omega_{p'}) \rho^{(\ell)}(\omega_{p'} - \omega_c) = 0 \quad . \quad (5.4)$$

The imaginary part of the coherent frequency, Ω_c , (with the negative sign) represents the inverse growth-time and is expressed by the following formula

$$\frac{1}{\tau^l} = -\frac{ce\beta I_0}{4\pi E v} \operatorname{Re} Z_{\text{eff}}^l, \quad (5.5)$$

where E is the total energy of a proton and Z_{eff}^l is the effective impedance defined as follows

$$Z_{\text{eff}}^l = \frac{2\pi}{l+1} \frac{1}{2\omega_0 \hat{\tau}} \sum_{p'=-\infty}^{\infty} Z_{\perp}(\omega_{p'}) \rho^l(\omega_{p'} - \omega_{\xi}) \quad (5.6)$$

The above result can be compared with the growth-time obtained in the framework of the Vlasov equation-based description of the slow head-tail instability. The so-called "air bag" model⁸ has exactly the same generic form as given by Eq.(5.5) with the effective impedance introduced as an average over a different set of spectral density functions; namely the Bessel functions of the first kind.

In order to evaluate the effective impedance, given by Eq.(5.6), one has to convolute the transverse impedance, evaluated in Sec.1, with the beam spectrum, Eq.(5.2). The result of the above summation obviously depends on chromaticity. The resistive wall contribution has already been discussed in Sec.4, therefore we will concentrate on the three remaining contributions to the coupling impedance, illustrated in Figs. 3a, 3b and 3c.

One can notice that both contributions (b) and (c) to the transverse impedance $Z_{\perp}(\omega)$, given by Eqs.(1.5)–(1.6) and Eqs.(1.7)–(1.8), have diffraction-like character (See Fig.3); a principle maximum of width $\lambda = \pi c/L$ at the origin and a series of equally spaced secondary maxima governed by the same width. Similarly, the harmonics of the beam spectrum, $\rho^l(\omega - \omega_{\xi})$, have one ($l=0$) or a pair ($l \geq 1$) of principle maxima of width $\varepsilon =$

$\pi/2\hat{\tau}$ followed by a sequence of secondary maxima (See Fig.19). Both spectra are sampled by a discrete set of frequencies, $\omega_p = (p + \nu)\omega_0$. In case of relatively long proton bunches ($2\hat{\tau} = 2 - 3 \times 10^{-9}$ sec) both widths λ and ε are comparable and they are of the order of the chromatic frequency, ω_{ξ} , evaluated at about 10 units of chromaticity.

These features combined with the convolution formula for the effective impedance,

result in substantial 'overlap' of the transverse impedance and the beam spectrum, which in turn leads to large values of effective impedance for relatively small chromaticities ($\xi \sim 10$).

In contrast, the effective impedance evaluated with the broad-band part of the transverse impedance (See Fig.3a) is much smaller than the one previously discussed. The last statement can be explained as follows; the width of the broad-band impedance peak, $\delta = \omega_c/Q$, is much larger than ϵ and in order to overlap this broad peak with the principal maximum of the power spectrum harmonics (to get a nonzero effective impedance) one would have to shift both spectra by ω_ξ of the order of δ . This, in turn, would require enormous values of the chromaticity ($\xi \sim 10^4$).

Summarizing, only two out of four contributions to the transverse impedance are relevant to the discussed coherent betatron instability. First, the kicker magnet contribution driving high frequency band of several lines centered around 500 MHz is in turn responsible for single bunch slow head-tail modes. The similar coupling due to the beam position monitors is much weaker, because of the small absolute value of the transverse impedance and therefore is neglected in further considerations.

Assuming only one dominant contribution to the transverse coupling impedance (due to the kicker magnets), the inverse growth-times were calculated numerically according to Eqs.(5.1)–(5.6). We also assume that the Tevatron, Main Ring and Main Injector have roughly the same kicker magnets contribution to the transverse impedance and the bunch intensity of 6×10^{10} ppb is used for the purpose of this model calculation. The resulting growth-rates as a function of chromaticity evaluated for different slow head-tail modes ($l=0, 1, 2, 3$) are illustrated for various operational modes of all three machines in Figs.20–22. Furthermore, the results of Figs.20–22 are summarized in Table 5. One can immediately see a qualitative difference between the $l=0$ and $l \geq 1$ modes; the $l=0$ mode is always stable for positive chromaticities, while the stability of the $l \geq 1$ modes strongly depends on chromaticity and longitudinal emittance

of the bunch. Table 5 collects extreme values of the characteristic growth-times, τ^l , for various slow head-tail modes, l , together with the values of chromaticity, ξ_{max} , corresponding to the most unstable points of the above modes. The Tevatron is dominated by the $l=1$ mode with the characteristic growth-time of about 20×10^{-3} sec., with the higher modes also displaying significant instability at their critical chromaticities (See Table 5). Our study shows that careful adjustment of chromaticity (avoiding its critical values, ξ_{max}) rather than increase of the longitudinal emittance may serve as an effective way of suppressing various modes of the coherent betatron instability in the Tevatron. On the other hand, low energy injection of short bunches to the Main Ring characterized by catastrophically unstable $l=1$ mode ($\tau^l = 2 \times 10^{-3}$ sec.) can be significantly improved by an increase of the longitudinal emittance. Emittance of 1.5 eV-sec. not only stabilizes the $l=1$ mode but also rises the growth-time of the dominant unstable $l=2$ mode to about 10×10^{-3} sec. In case of the Main Injector, which already performs much better for small emittances (the $l=1$ mode stable and the growth-time of the dominant unstable mode of about 10×10^{-3} sec.) the above cure is even more miraculous – it simultaneously stabilizes $l=2$ and 3 modes. This last superior feature of the Main Injector (compared to the Main Ring) can easily be explained by a larger chromatic frequency shift, ω_ξ , which governs ‘overlap’ of the beam spectrum and the driving transverse impedance, for a smaller storage ring ($\omega_\xi \sim R^{-1}$).

As far as more conventional cures are concerned, the active damper obviously does not work in case of the higher modes, since its feedback system picks up only the transverse position of a bunch centroid, which remains zero due to the symmetry of the higher modes. Another possible cure (also effective for the $l \geq 1$ modes) would involve the Landau damping through the octupole-induced betatron tune spread. Increasing betatron amplitude of initially unstable mode causes increase of the tune spread, which will eventually self-stabilize development of this mode.

ϵ [eV-sec.]	ν_{β}	l	ξ_{\max}	τ^l [sec]
Tevatron (p-injection) @ 150 GeV, $N_b = 6 \times 10^{10}$ ppb				
0.3	19.456	1	10	19×10^{-3}
		2	18	29×10^{-3}
		3	25	42×10^{-3}
1.5	19.456	1	3	20×10^{-3}
		2	10	25×10^{-3}
		3	15	32×10^{-3}
Main Ring (p-injection) @ 8.9 GeV, $N_b = 6 \times 10^{10}$ ppb				
0.3	19.4	1	18	2.9×10^{-3}
		2	12	6.7×10^{-3}
		3	30	5.2×10^{-3}
1.5	19.4	1	stable mode	
		2	15	10×10^{-3}
		3	8	95×10^{-3}
Main Injector (p-injection) @ 8.9 GeV, $N_b = 6 \times 10^{10}$ ppb				
0.3	22.6	1	stable mode	
		2	16	2.5×10^{-3}
		3	14	5.1×10^{-3}
1.5	22.6	1	stable mode	
		2	stable mode	
		3	stable mode	

Table 5

6. CONCLUSIONS

Our survey of possible intensity limitations due to the coherent phenomena can be summarized through the following list of conclusions and recommendations.

The microwave instability in the high energy region (Tevatron injection) seems to be dominated by the broad-band impedance contribution. As established in Sec. 2, the Tevatron's thresholds are not very restrictive (especially the transverse one), therefore one should not expect any danger of the microwave instability; even for very short bunches ($\sigma_L \sim 10^{-1}$ m) and small transverse emittances ($\epsilon \sim 1$ mm mrad), as long as the bunch intensities do not significantly exceed 10^{11} ppb. On the other hand, in case of low energy injection to the Main Ring or Main Injector (@ 8.9 GeV) the microwave instability is virtually dominated by the coherent space-charge force, and therefore the beam size (transverse emittance) strongly affects the intensity thresholds. Even so, for rather small emittance of $\epsilon \sim 1$ mm mrad and a very short bunch-length of $\sigma_L \sim 10^{-1}$ m, the beam should safely withstand the bunch intensity of 3×10^{10} ppb. Furthermore, our study shows that the beam, unstable exactly at the transition, quickly gains stability shortly after the transition crossing. Comparison between the Main Ring and the Main Injector shows slightly higher intensity thresholds and faster recovery after the transition crossing for the Main Injector, nevertheless both machines test quite well against the microwave instability, which does not seem to pose any danger for intensities smaller than 10^{11} ppb.

The colliding mode instability thresholds are even less restrictive, both in low energy (Tevatron) and high energy (Main Ring, Main Injector) regions. The transverse threshold is always about two orders of magnitude lower than the longitudinal one, and still the transverse colliding mode instability is safe below intensities of 10^{12} ppb. The instability thresholds weakly depend on energy and the transition crossing for all cases considered here.

Finally a case of the transverse multi-bunch instability due to resistive wall impedance was considered; for both the fixed target and multi-bunch collider operational modes. We concluded, that for the high intensity fixed target scenario ($N_b = 5 \times 10^{10}$ ppb) the injection to the Tevatron is limited by the transverse instability with the characteristic growth-time of about 30 msec. , which can easily be suppressed by a feedback system. On the other hand, the same high intensity injection to the Main Ring faces very fast transverse instability with the growth-time order of magnitude shorter than the characteristic growth-time of the Tevatron's instability at injection. This may pose a serious problem for an active damper and one may have to resort to a strong Landau damping decoherence scheme eg. octupole tune spread, which may be able to suppress the instability. The Main Injector design seems to be quite resistant to the transverse coupled bunch instability; even for high intensity injection the characteristic growth-time is about 12 msec., which may be handled by a fast feedback system. For the new collider mode with 96 on 96 high intensity bunches ($N_b = 5 \times 10^{10}$), the communication between bunches is quite significant and it yields to the growth-time of about 300 msec., which may call for a damper system for the collider mode as well.

Finally, we have examined a high frequency (500 – 900 MHz region), single-bunch transverse instability, known as the slow head-tail instability⁷. The instability was first observed⁶ during the recent 1987–88 Tevatron fixed target run as a rapidly developing coherent betatron motion, resulting in a significant emittance growth, which limits machine performance and in a catastrophic scenario it even prevents extraction of the beam. One obviously expects, that even more pronounced version of this instability will be present in the proposed high-intensity upgrades, therefore one should examine its prospective strength in the Tevatron, Main Ring and the Main Injector.

Assuming only one dominant contribution to the transverse coupling impedance (due to the kicker magnets), the inverse growth-times were calculated numerically according to Eqs.(5.1)–(5.6). We also assume that the Tevatron, Main Ring and Main

Injector have roughly the same kicker magnets contribution to the transverse impedance and the bunch intensity of 6×10^{10} ppb is used for the purpose of this model calculation. The resulting growth-rates as a function of chromaticity evaluated for different slow head-tail modes ($l=0, 1, 2, 3$) are illustrated for various operational modes of all three machines in Figs.20–22. Furthermore, the results of Figs.20–22 are summarized in Table 5. One can immediately see a qualitative difference between the $l=0$ and $l \geq 1$ modes; the $l=0$ mode is always stable for positive chromaticities, while the stability of the $l \geq 1$ modes strongly depends on chromaticity and longitudinal emittance of the bunch. Table 5 collects extreme values of the characteristic growth-times, τ^l , for various slow head-tail modes, l , together with the values of chromaticity, ξ_{\max} , corresponding to to the most unstable points of the above modes. The Tevatron is dominated by the $l=1$ mode with the characteristic growth-time of about 20×10^{-3} sec., with the higher modes also displaying significant instability at their critical chromaticities (See Table 5). Our study shows that careful adjustment of chromaticity (avoiding its critical values, ξ_{\max}) rather than increase of the longitudinal emittance may serve as an effective way of suppressing various modes of the coherent betatron instability in the Tevatron. On the other hand, low energy injection of short bunches to the Main Ring characterized by catastrophically unstable $l=1$ mode ($\tau^l=2 \times 10^{-3}$ sec.) can be significantly improved by the increase of the longitudinal emittance. Emittance of 1.5 eV-sec. not only stabilizes the $l=1$ mode but also rises the growth-time of the dominant unstable, $l=2$, mode to about 10×10^{-3} sec. In case of the Main Injector, which already performs much better for small emittances (the $l=1$ mode is stable and the growth-time of the dominant unstable mode is of about 10×10^{-3} sec.) the above cure is even more miraculous; it simultaneously stabilizes $l=2, 3$ modes. This last superior feature of the Main Injector (compared to the Main Ring) can easily be explained by a larger chromatic frequency shift, ω_ξ , which governs 'overlap' of the beam spectrum and the driving transverse impedance, for a smaller storage ring ($\omega_\xi \sim R^{-1}$).

As far as more conventional cures of the coherent betatron instabilities are concerned, the active damper obviously does not work in case of the higher modes, since its feedback system picks up only the transverse position of a bunch centroid, which remains zero due to the symmetry of the higher modes. Another possible cure (also effective for the $l \geq 1$ modes) would involve the Landau damping through the octupole-induced betatron tune spread. Increasing betatron amplitude of initially unstable mode causes increase of the tune spread, which will eventually self-stabilize development of this mode.

One should emphasize that the above study does not take into account decohering effects of the Landau damping resulting from various tune spreads present in any more realistic coherent instability model. Our results are, therefore, overestimated and may serve as the worst possible scenarios. It may be desirable to include the Landau damping to obtain less stringent thresholds and to implement it as a way of suppressing the coherent instabilities.

ACKNOWLEDGEMENT

I wish to thank Mike Harrison and Dave Finley for bringing to my attention new aspects of the upgrades, possibly relevant to the coherent instability problem and for furnishing the upgrade design parameters. I would also like to thank Chuck Ankenbrandt for suggesting to include new features of the Main Injector into this study. Finally, I wish to acknowledge stimulating discussions with Bill Ng and Craig Moore.

REFERENCES

1. T. Weiland, DESY 82-015, (1982)
2. K.Y. Ng, Principles of the High Energy Hadron Colliders, Part I: The SSC, edited by A.W. Chao and M. Month
3. K.Y. Ng, FERMILAB TM-1388, (1986)
4. S. Krinsky and J.M. Wang, Particle Accelerators **17**, 109, (1985)
5. G. Guignard, Selection of Formulae concerning Proton Storage Rings, CERN 77-10, (1977)
6. S.A. Bogacz, M. Harrison and K.Y. Ng, FERMILAB FN-485, (1988)
7. F. Sacherer, Proc. 9-th Int. Conf. on High Energy Accelerators, Stanford 1974, p. 347
8. F. Sacherer, CERN/SI-BR/72-5 (1972), unpublished

FIGURE CAPTIONS

- Fig. 1 TBCI simulation of the longitudinal and transverse impedance of the Tevatron bellow (a single unit consisting of 24 ripples)
- Fig. 2 Longitudinal impedance of the Tevatron – selected contributions
- Fig. 3 Transverse impedance of the Tevatron – selected contributions
- Fig. 4 Tevatron's coupling impedance – summary
- Fig. 5 Longitudinal impedance, $|Z_{||}/n|$, of the Tevatron – net result
- Fig. 6 Microwave Instability – longitudinal and transverse intensity thresholds (Tevatron, injection, $\sigma_t = 0.3$ m)
- Fig. 7 Microwave Instability – longitudinal and transverse intensity thresholds (Tevatron, injection, $\sigma_t = 0.1$ m)
- Fig. 8 Microwave Instability – longitudinal and transverse intensity thresholds (Main Ring, injection, $\sigma_t = 0.3$ m)
- Fig. 9 Microwave Instability – longitudinal and transverse intensity thresholds (Main Ring, storage, $\sigma_t = 0.3$ m)
- Fig. 10 Microwave Instability – longitudinal and transverse intensity thresholds (Main Injector, injection, $\sigma_t = 0.3$ m)
- Fig. 11 Microwave Instability – longitudinal and transverse intensity thresholds (Main Injector, storage, $\sigma_t = 0.3$ m)
- Fig. 12 Colliding Mode Instability – longitudinal and transverse intensity thresholds (Tevatron, injection, $\sigma_t = 0.3$ m)
- Fig. 13 Colliding Mode Instability – longitudinal and transverse intensity thresholds (Main Ring, $\sigma_t = 0.3$ m)

- Fig. 14 Colliding Mode Instability – longitudinal and transverse intensity thresholds (Main Injector, $\sigma_l = 0.3$ m)
- Fig. 15 Resistive Wall Instability – growth-time vs betatron tune (Tevatron, fixed target and collider modes, $\sigma_l = 0.3$ m)
- Fig. 16 Resistive Wall Instability – growth-time vs betatron tune (Main Ring, injection, $\sigma_l = 0.3$ m)
- Fig. 17 Resistive Wall Instability – growth-time vs betatron tune (Main Injector, injection, $\sigma_l = 0.3$ m)
- Fig. 18 Transverse resistive wall impedance vs betatron tune (Tevatron, Main Ring and Main Injector)
- Fig. 19 Harmonics of the beam power spectrum $\rho_f(\omega)$. Markers denote the sampling frequencies $\omega_p = \omega_0(p + \nu)$. Dimensionless frequency is given in units of $x = \omega/\omega_0$
- Fig. 20 Tevatron – a family of inverse growth-time vs chromaticity curves evaluated numerically for various head-tail mode indices l
- Fig. 21 Main Ring – a family of inverse growth-time vs chromaticity curves evaluated numerically for various head-tail mode indices l
- Fig. 22 Main Injector – a family of inverse growth-time vs chromaticity curves evaluated numerically for various head-tail mode indices l

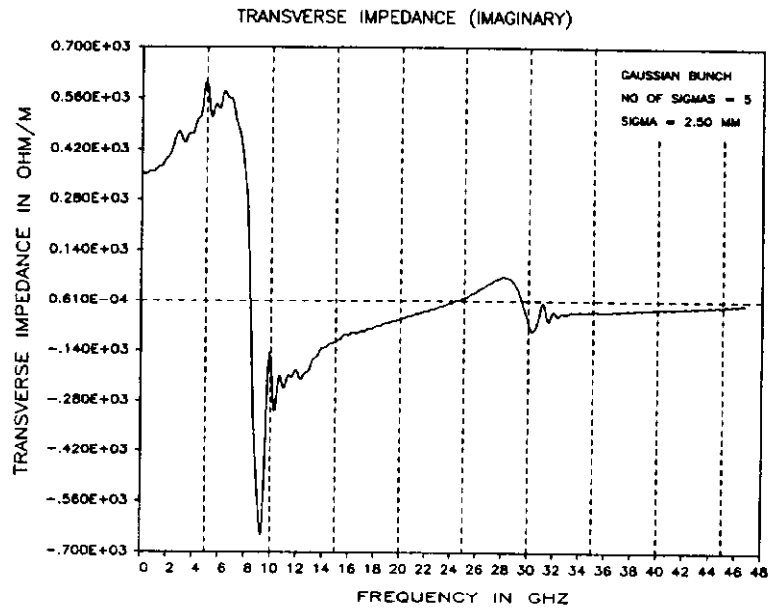
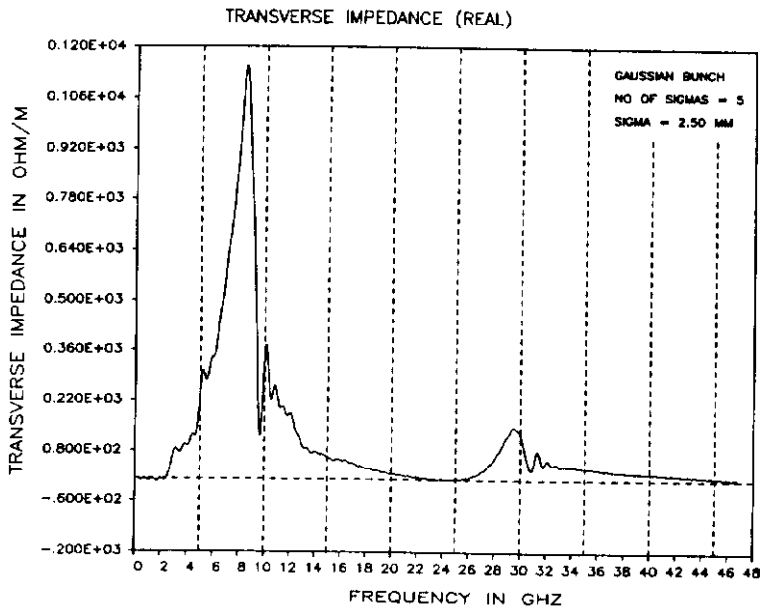
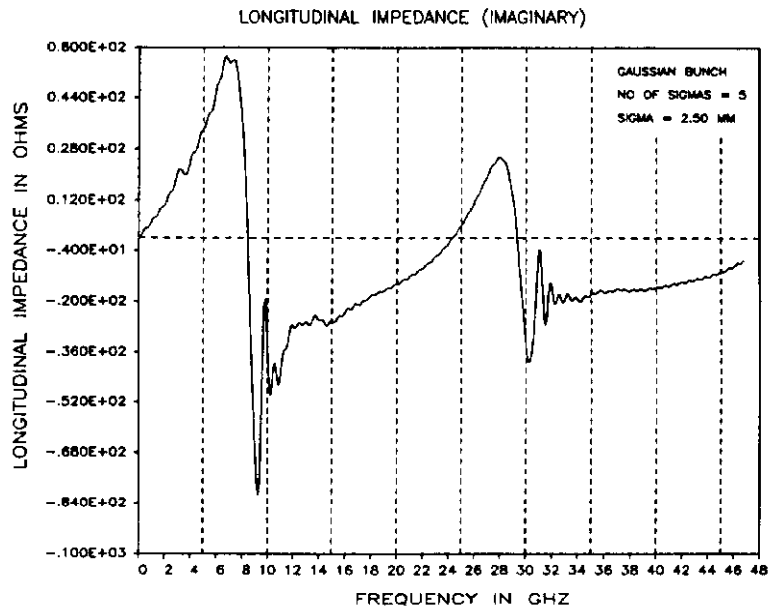
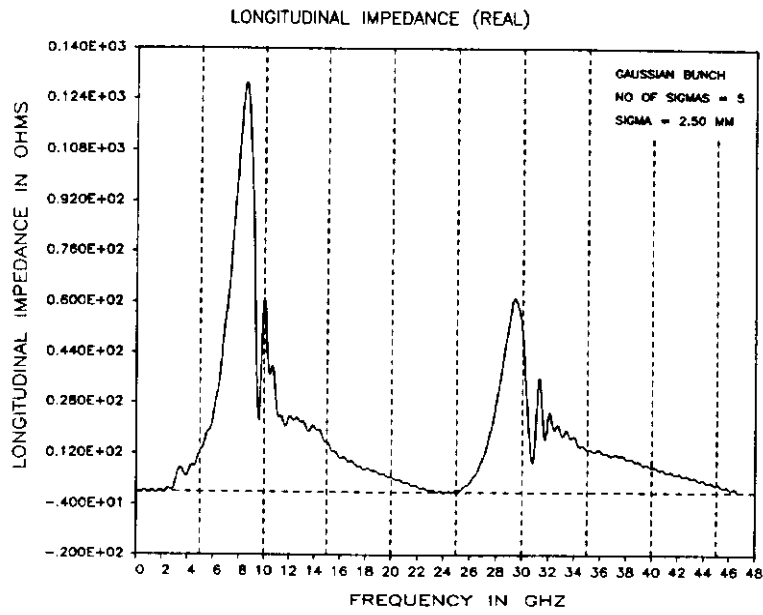
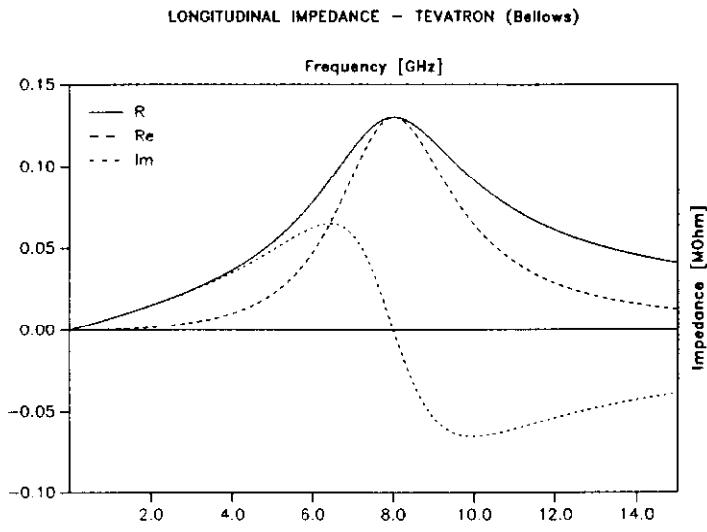
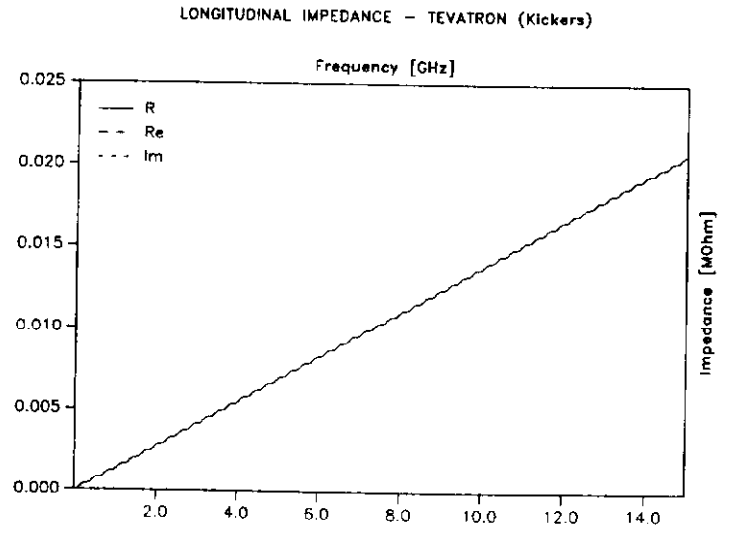


Fig. 1

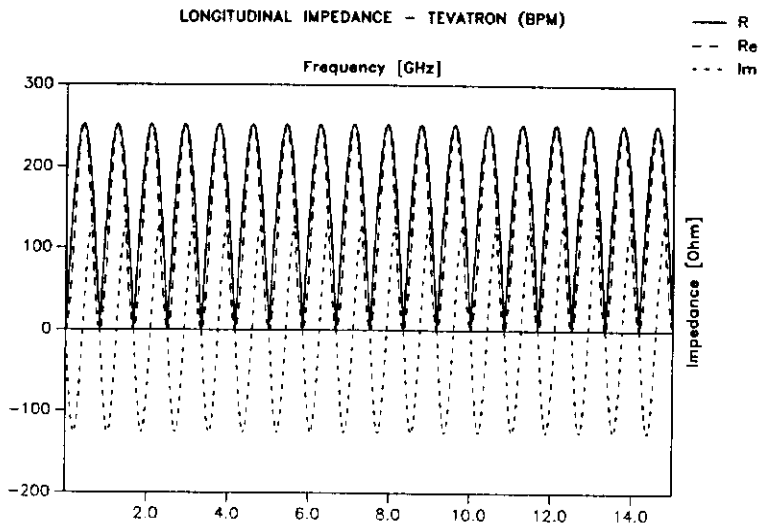
a)



b)



c)



d)

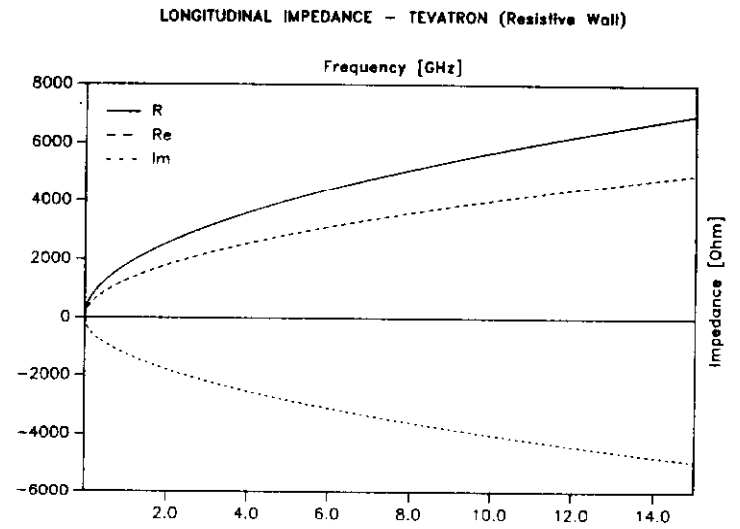
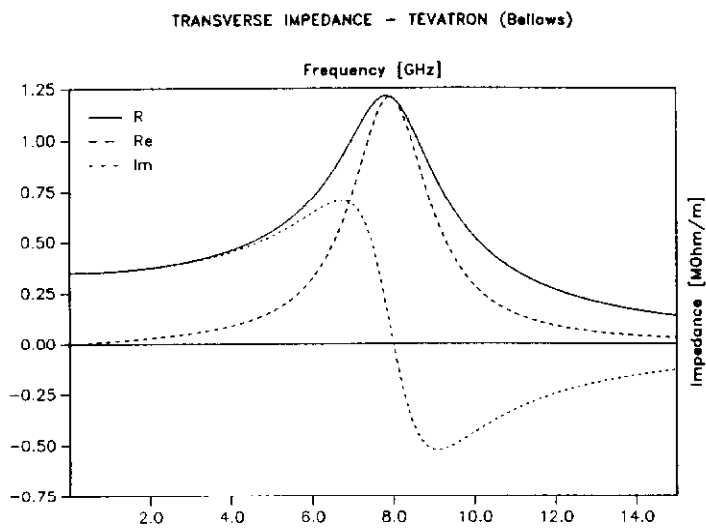
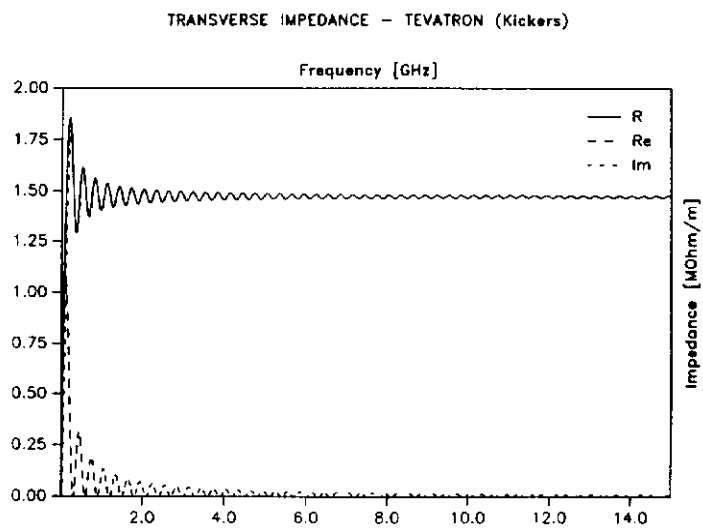


Fig. 2

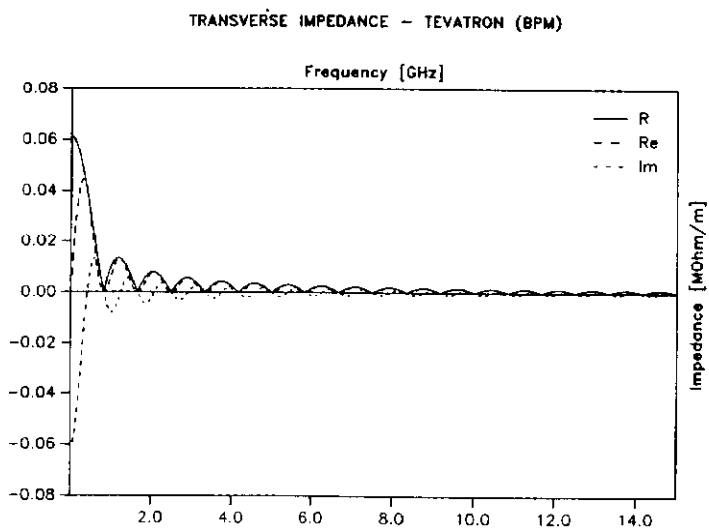
a)



b)



c)



d)

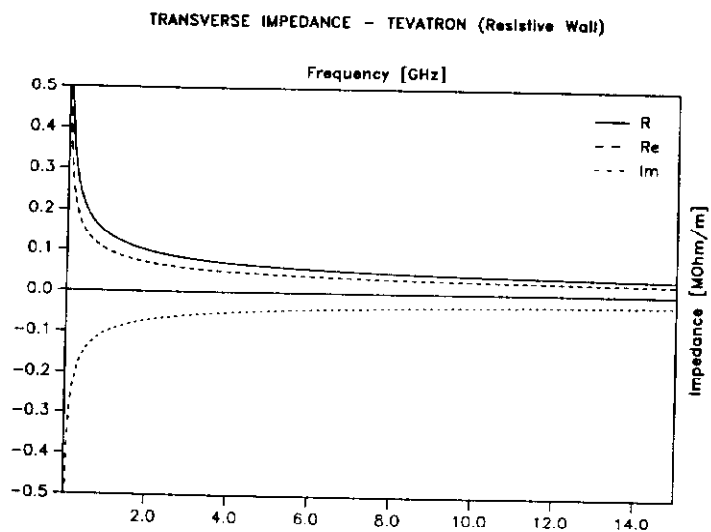
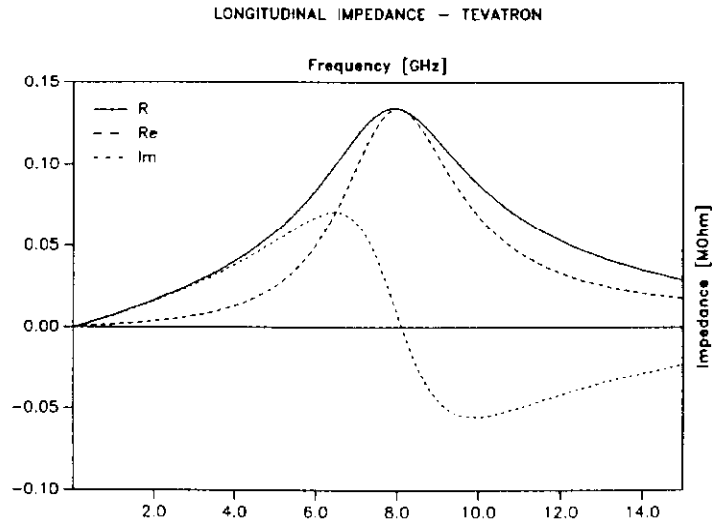


Fig. 3

a)



b)

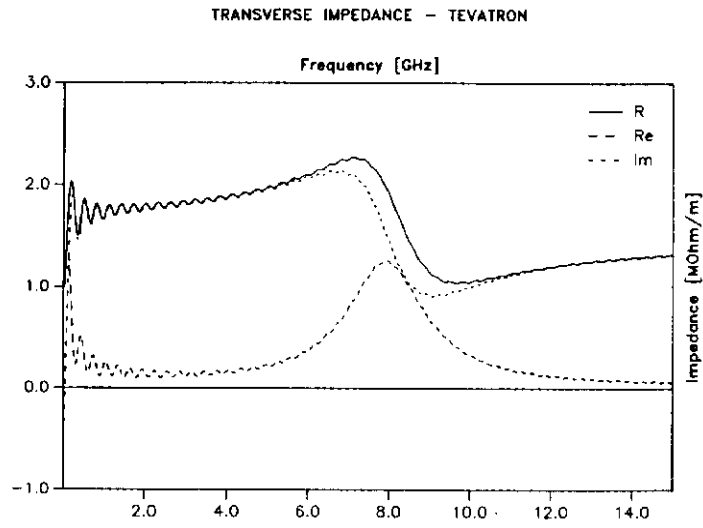


Fig. 4

LONGITUDINAL IMPEDANCE $|Z/n|$

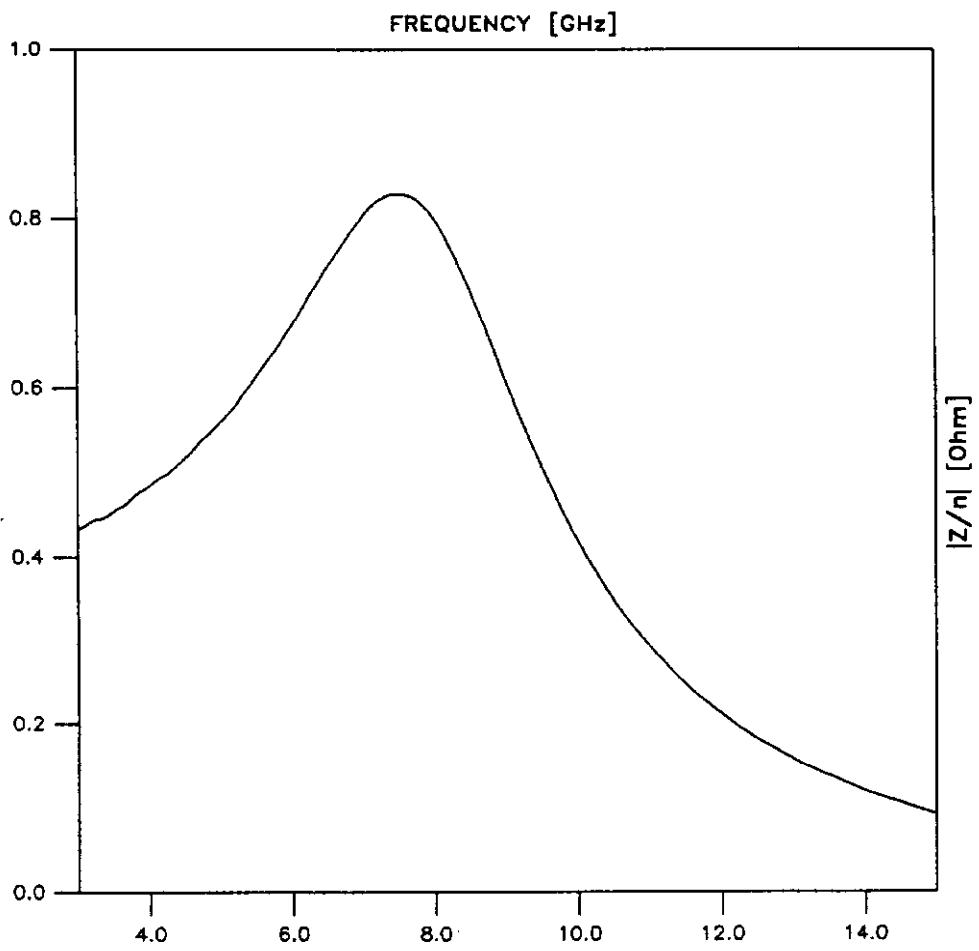


Fig. 5

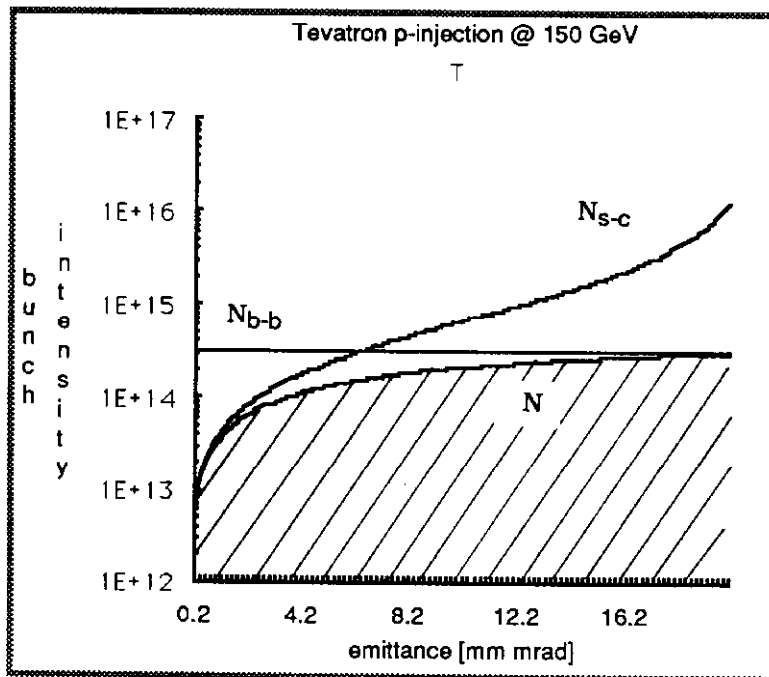
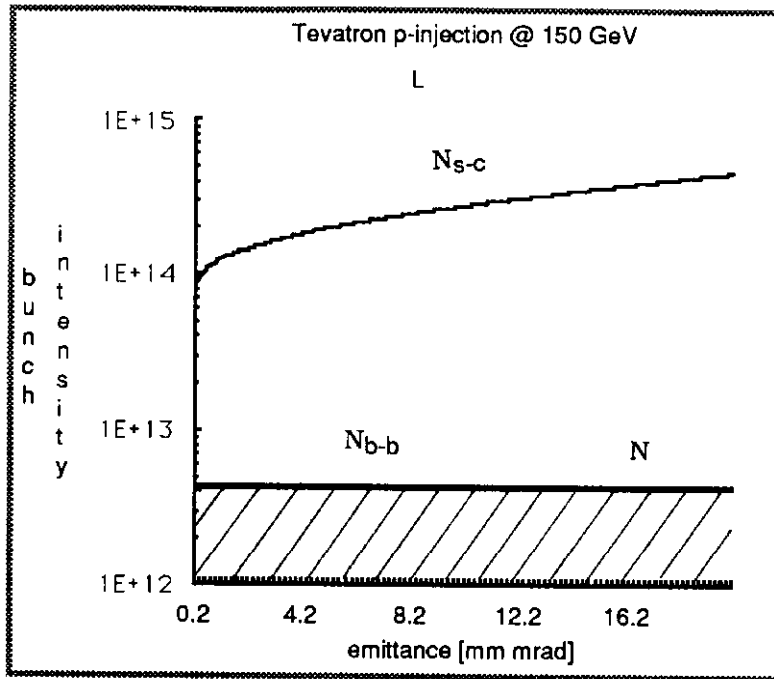


Fig.6

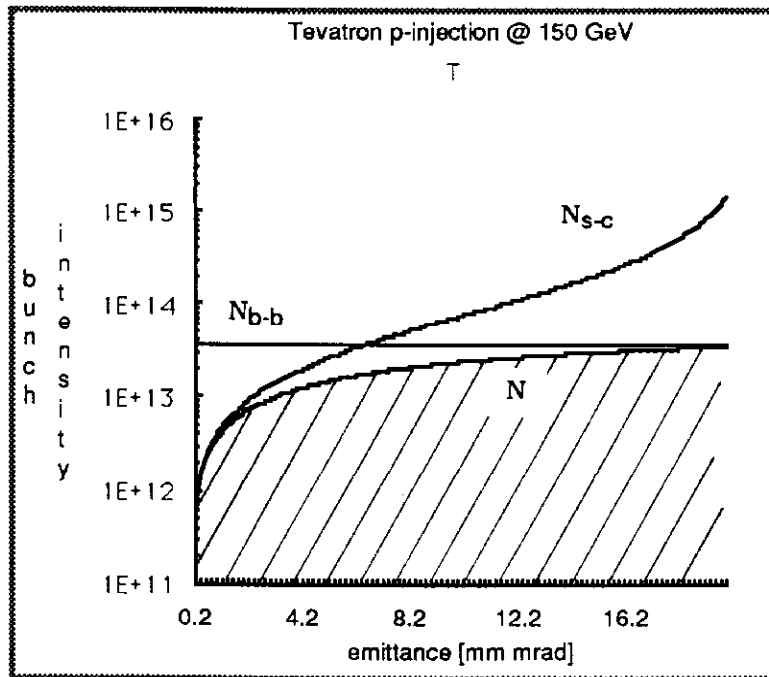
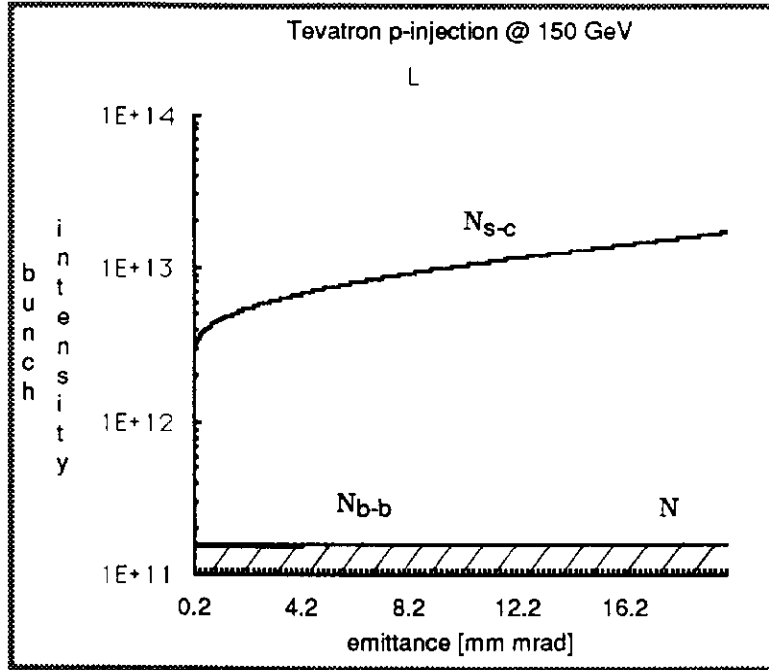


Fig.7

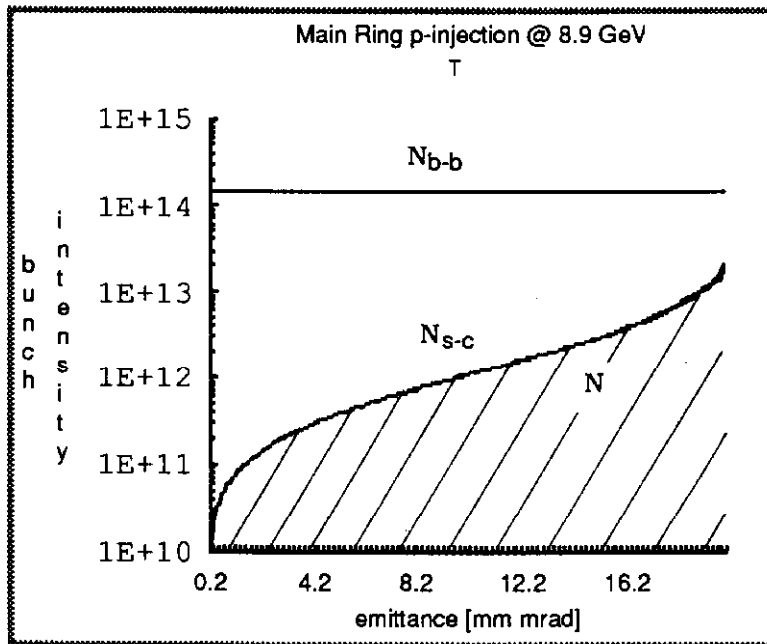
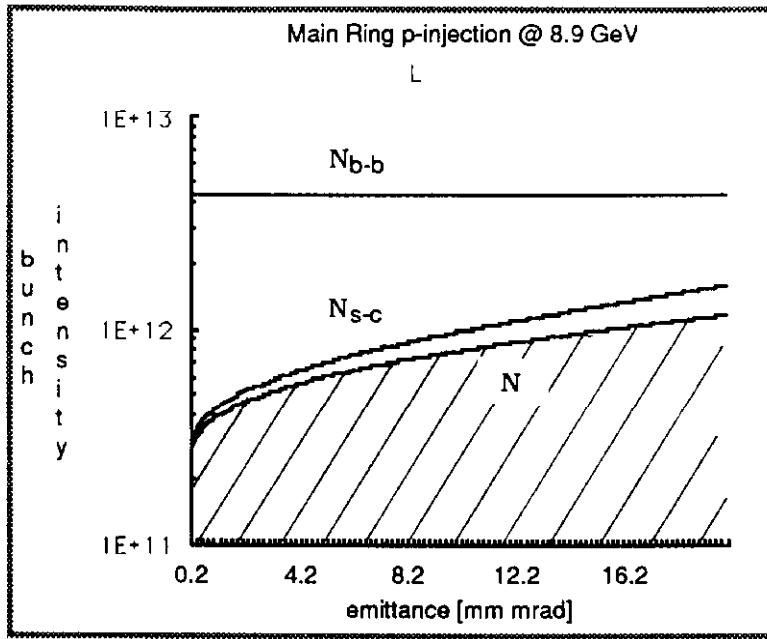


Fig.8

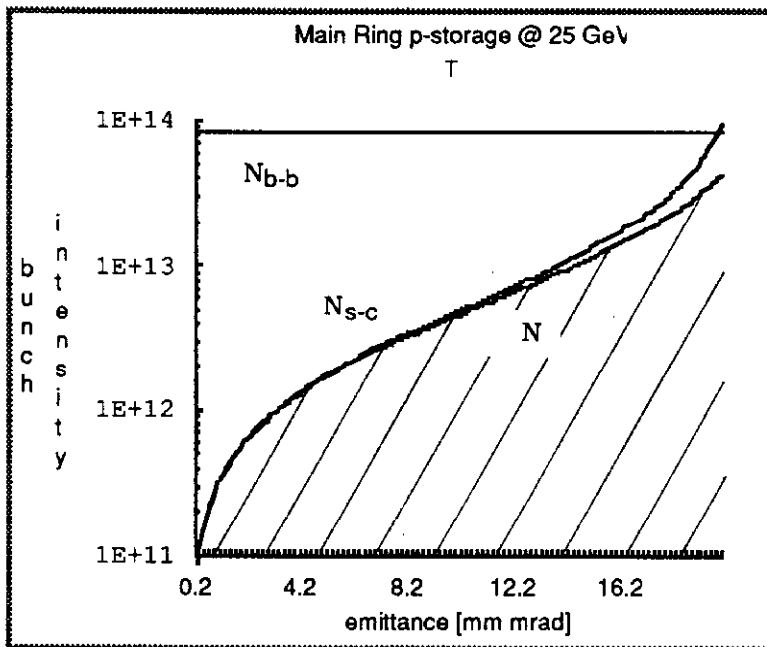
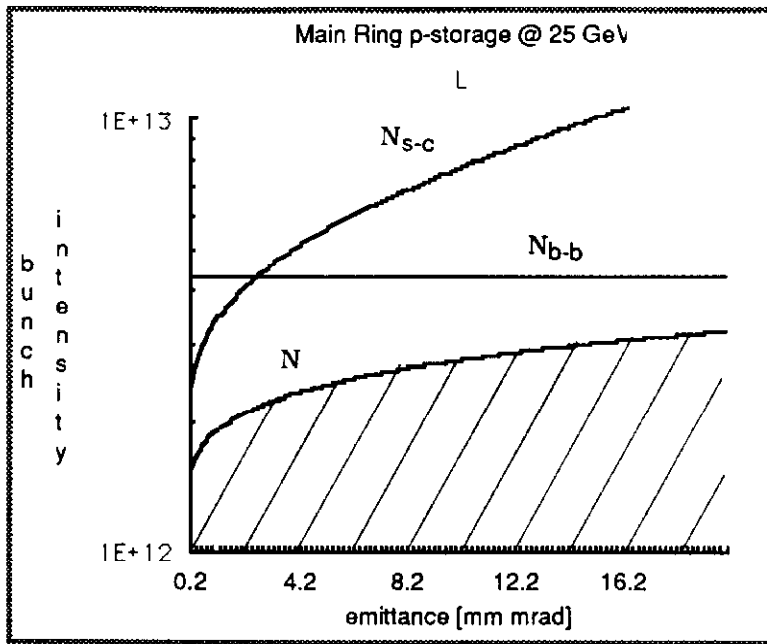


Fig.9

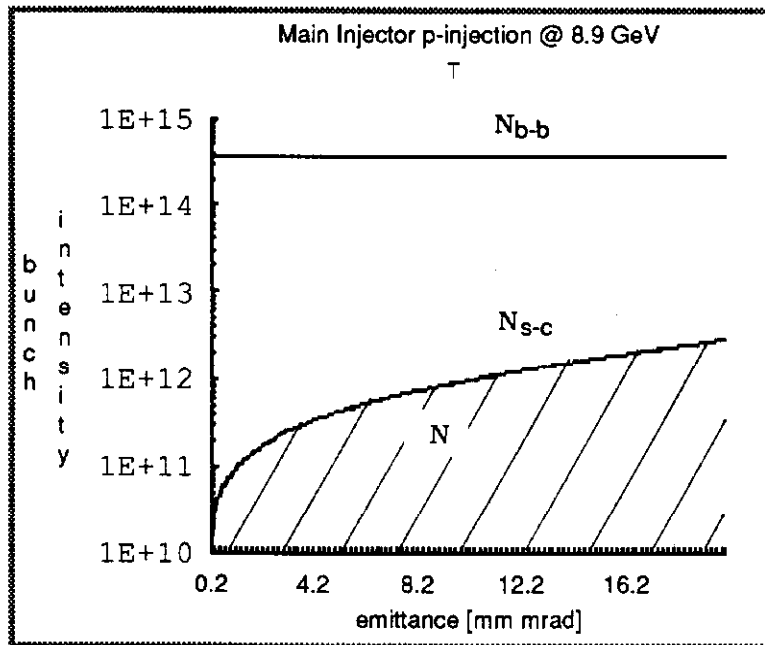
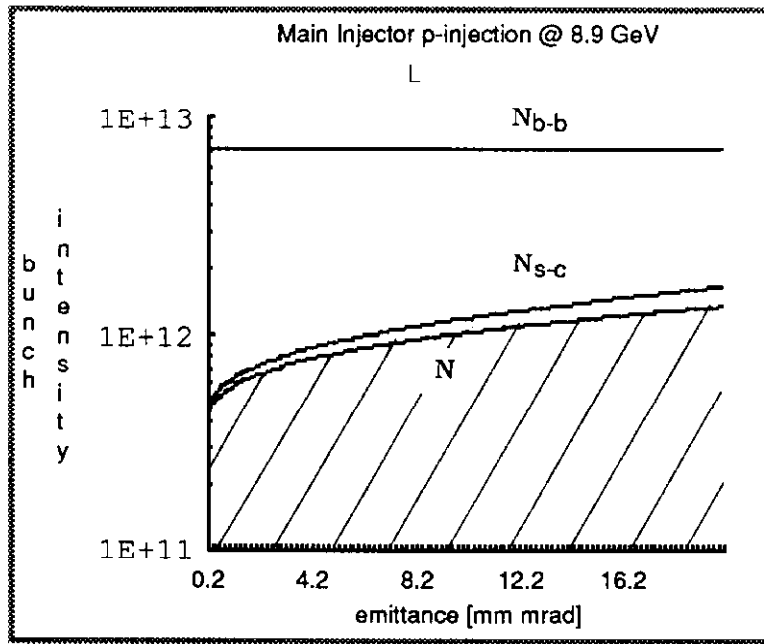


Fig.10

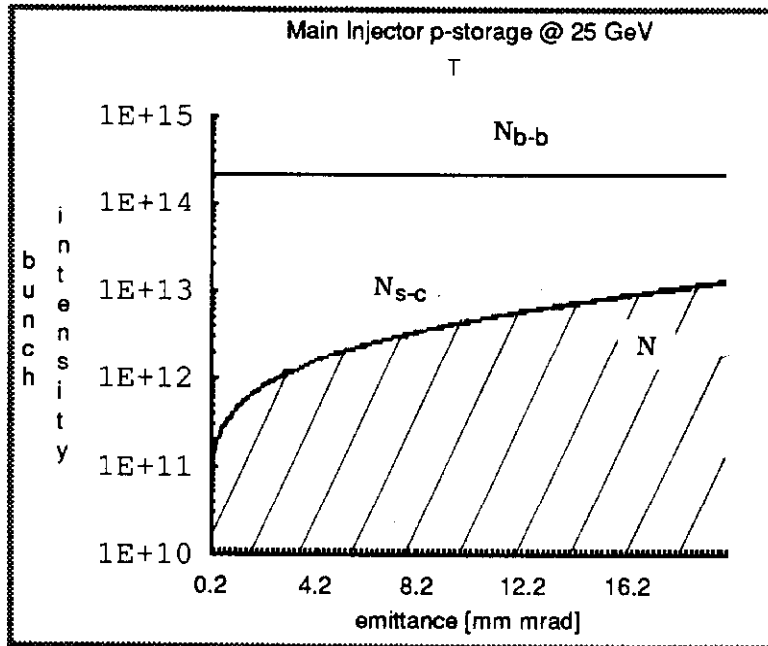
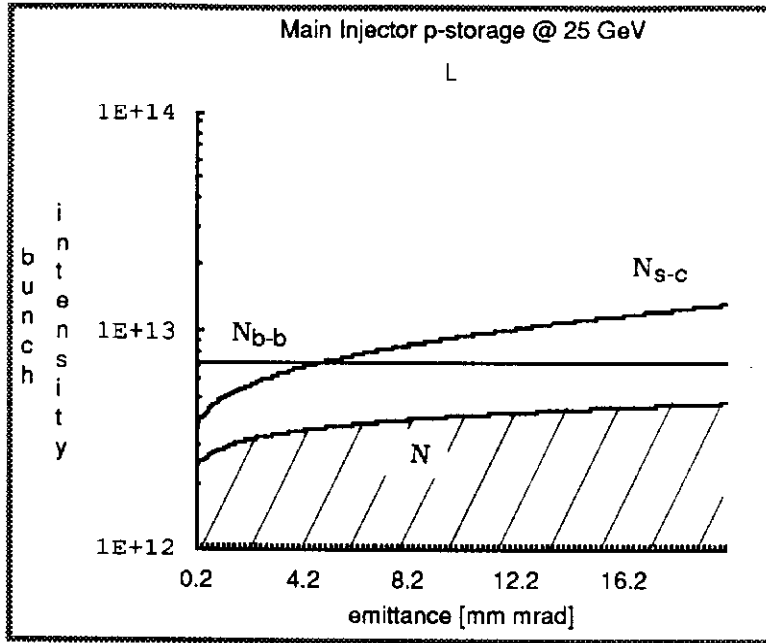


Fig.11

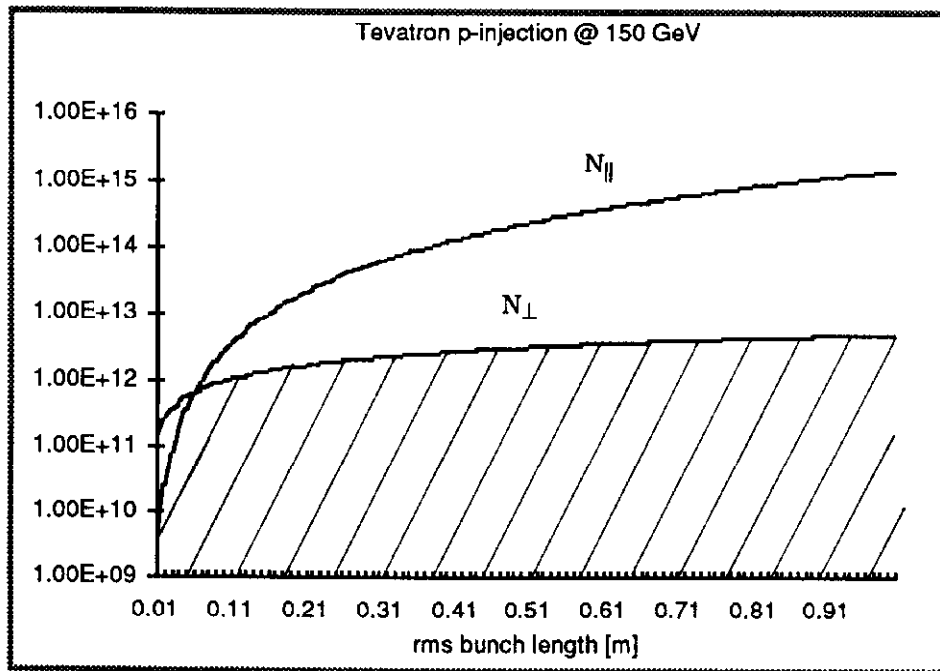


Fig. 12

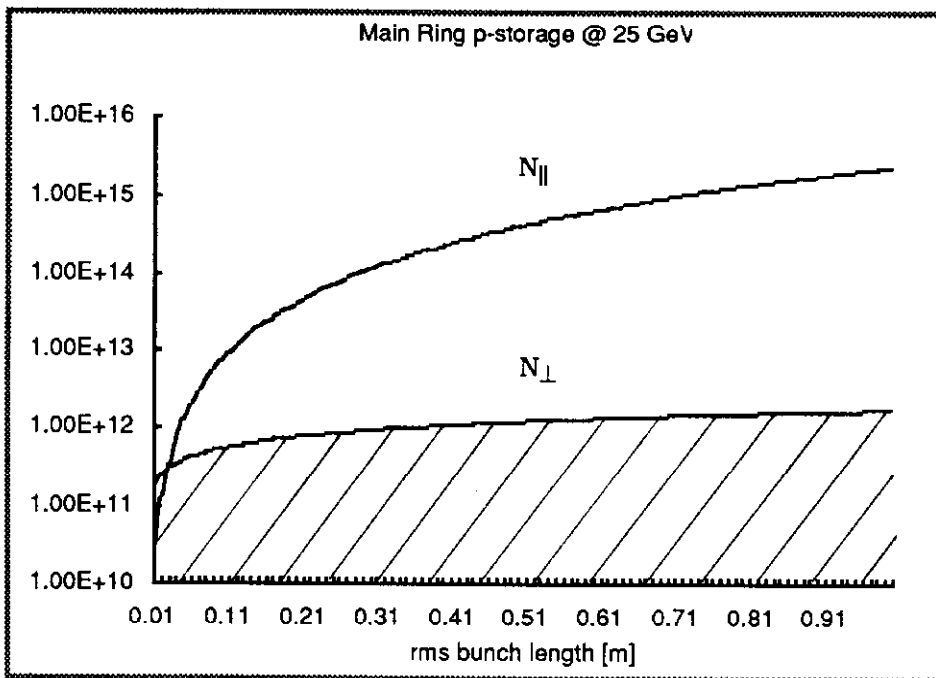
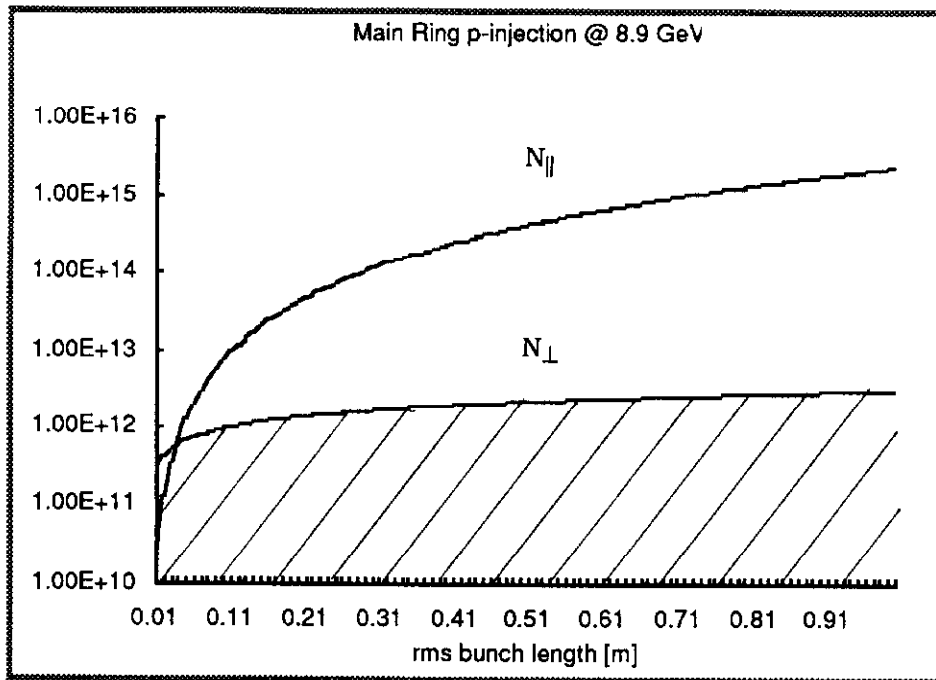


Fig.13

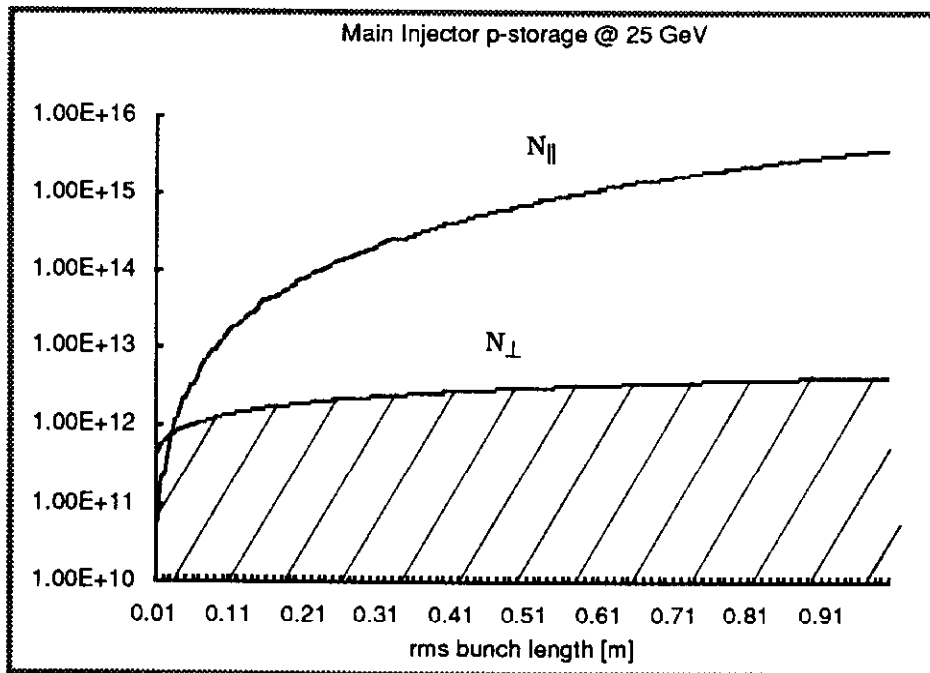
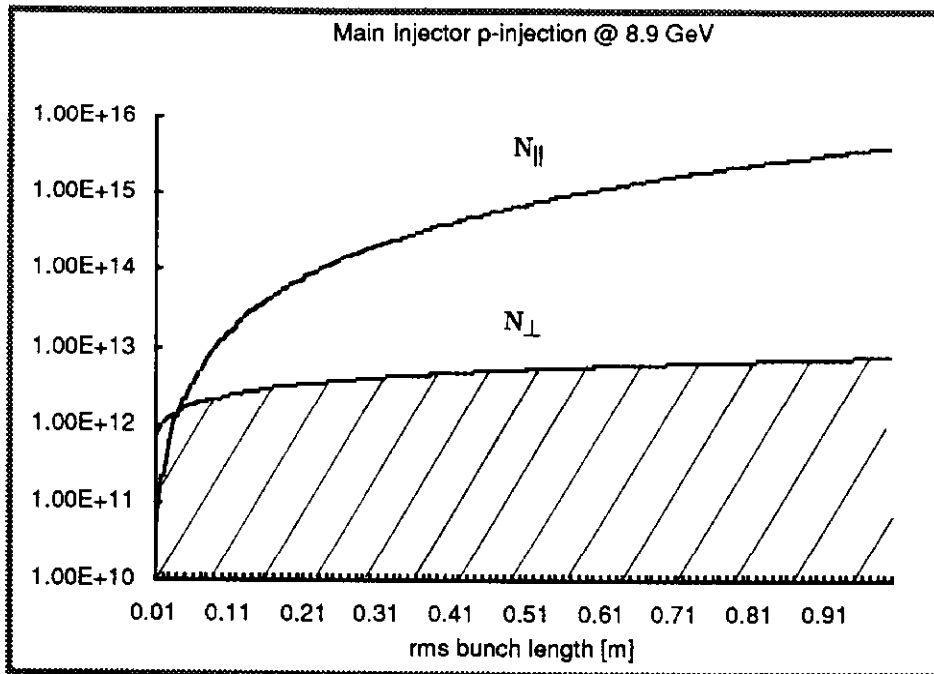


Fig.14

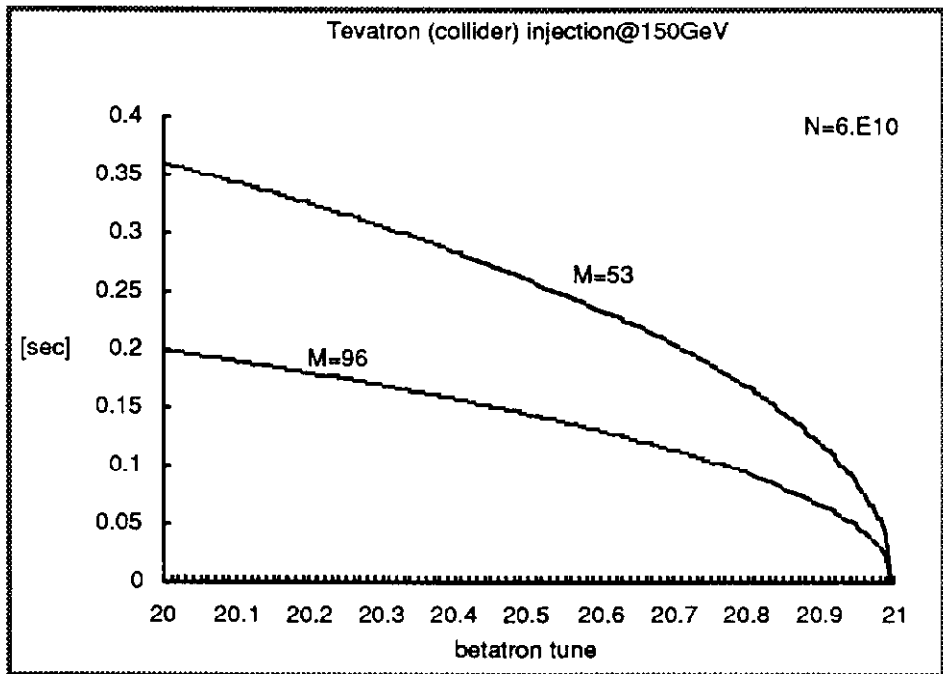
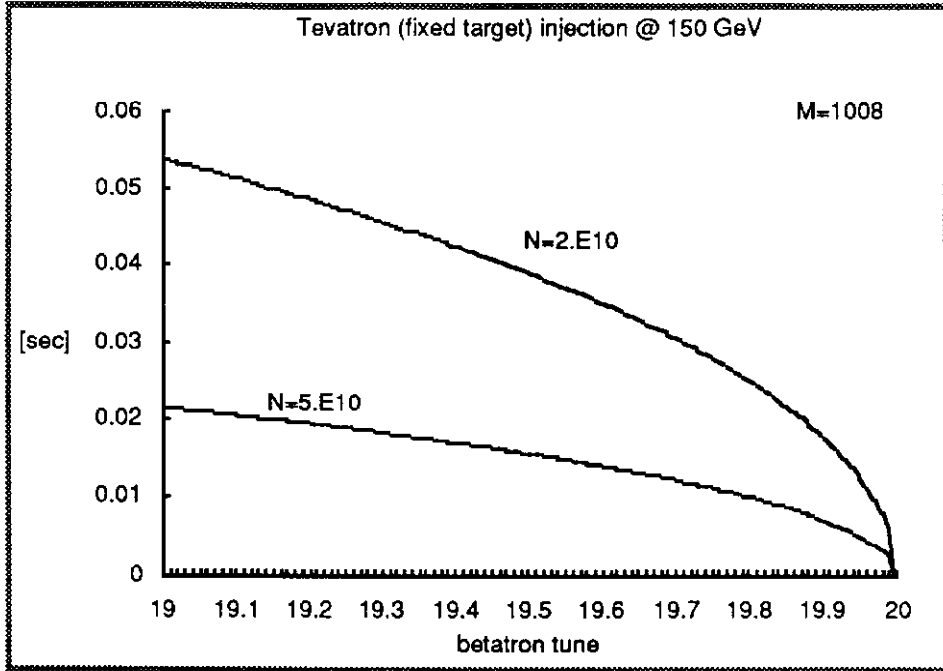


Fig. 15

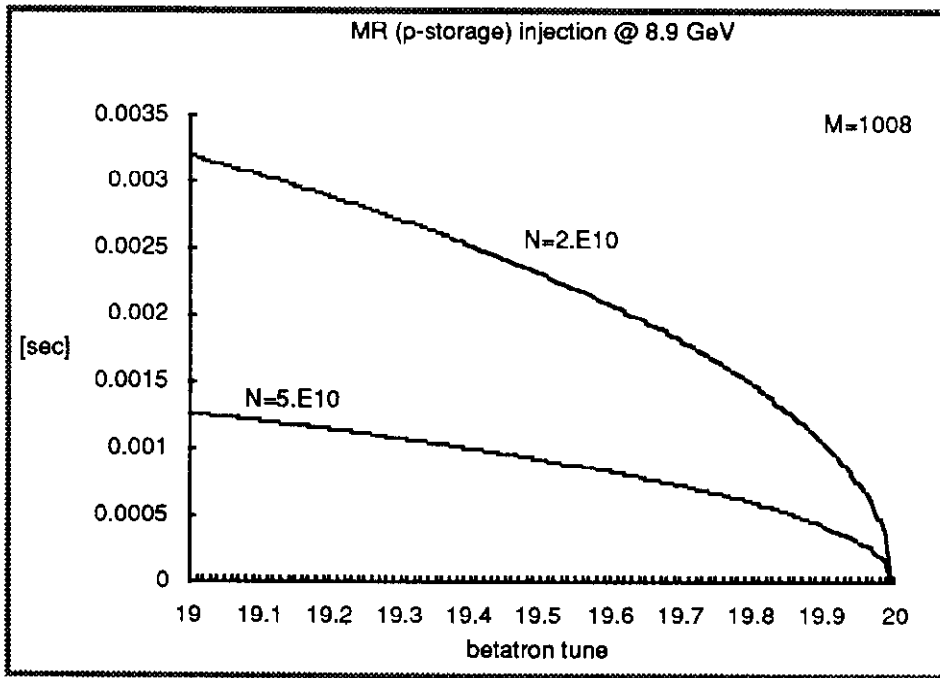


Fig.16

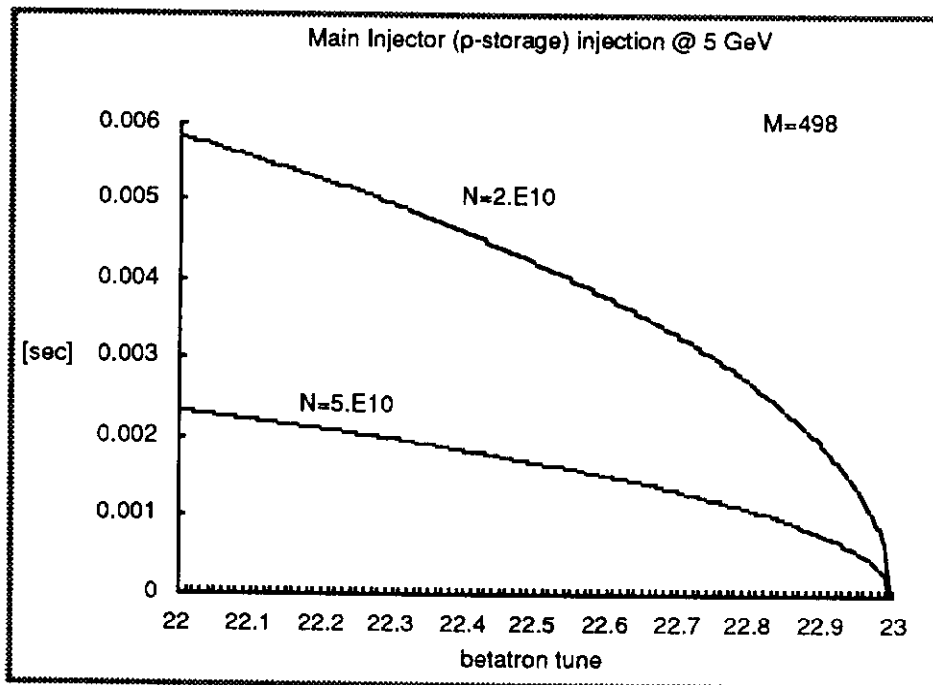
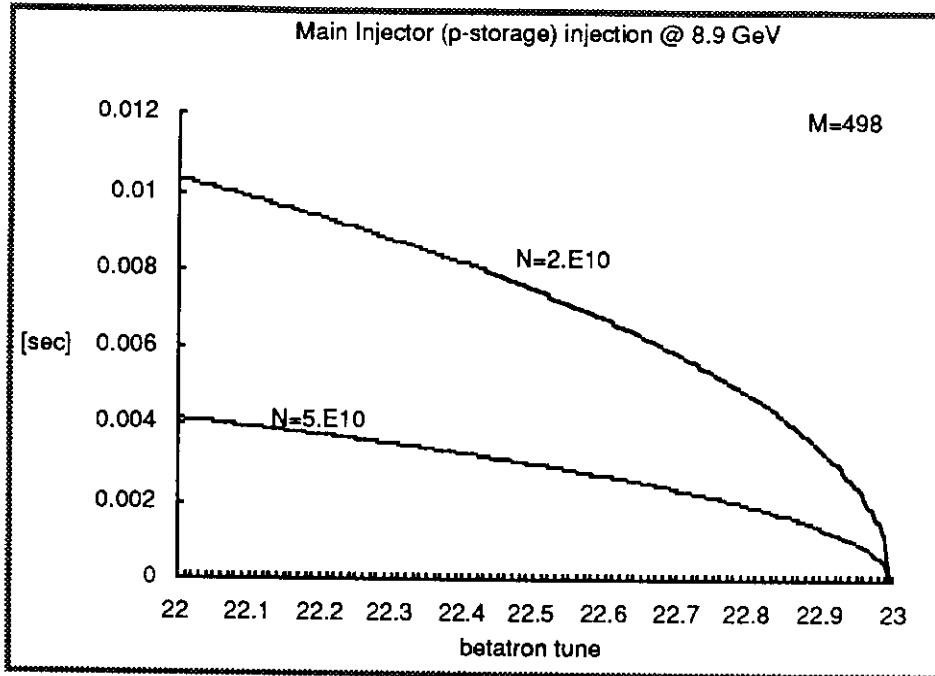


Fig.17

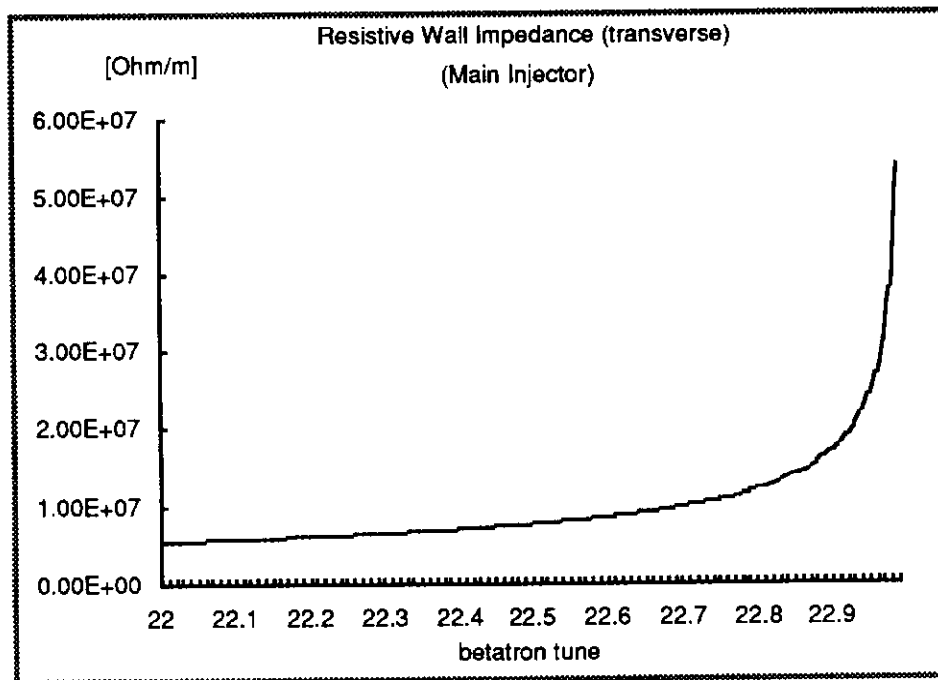
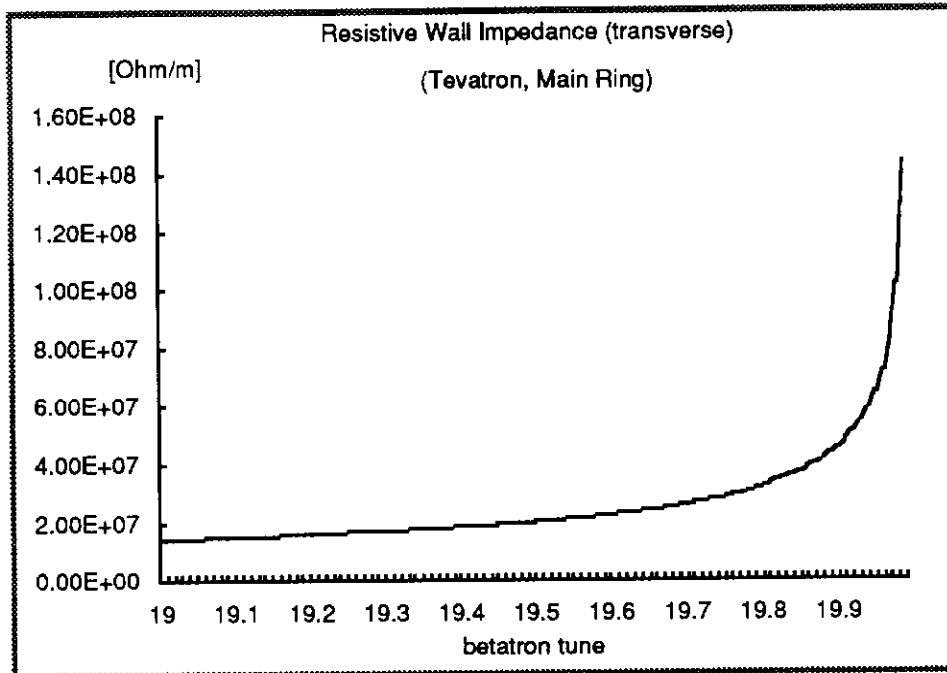


Fig.18

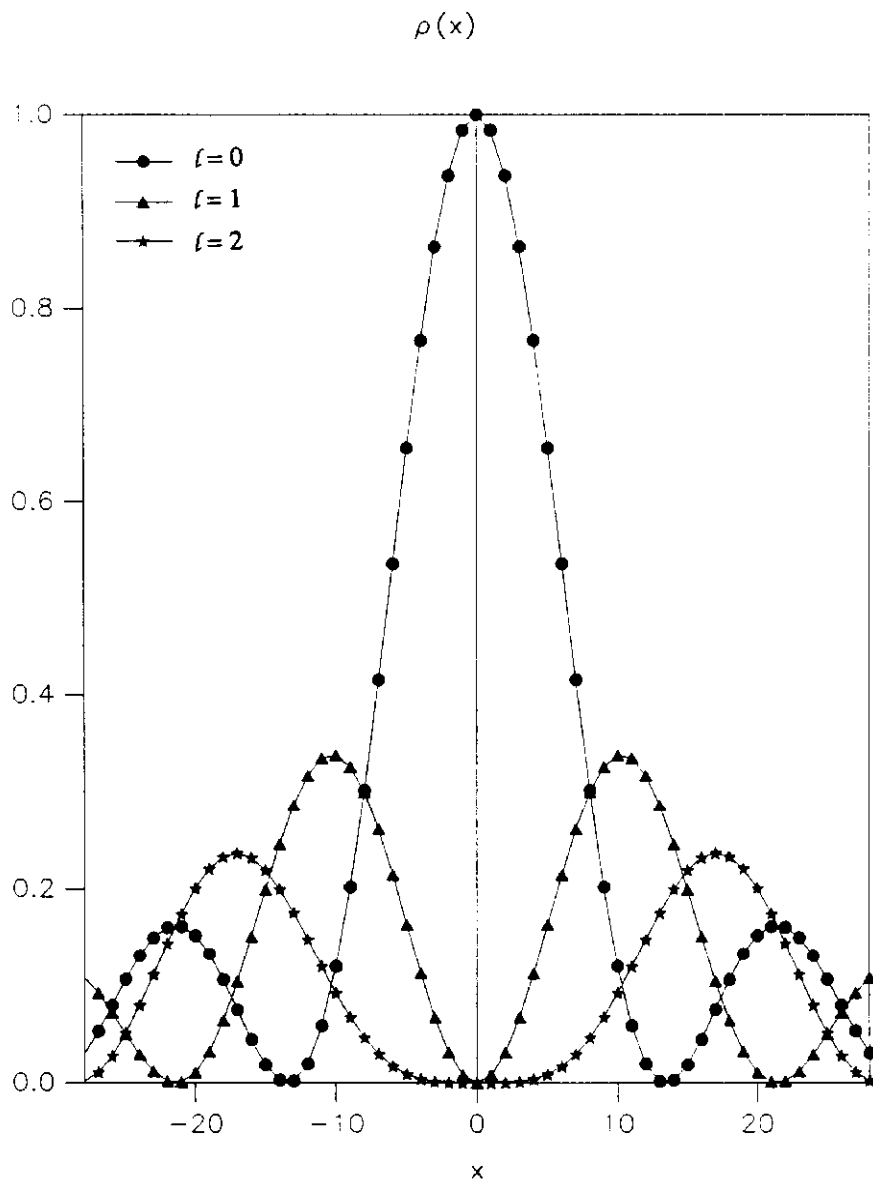


Fig. 19

Tevatron (fixed target) p-injection @ 150 GeV

$\epsilon = 0.3$ eV-sec.

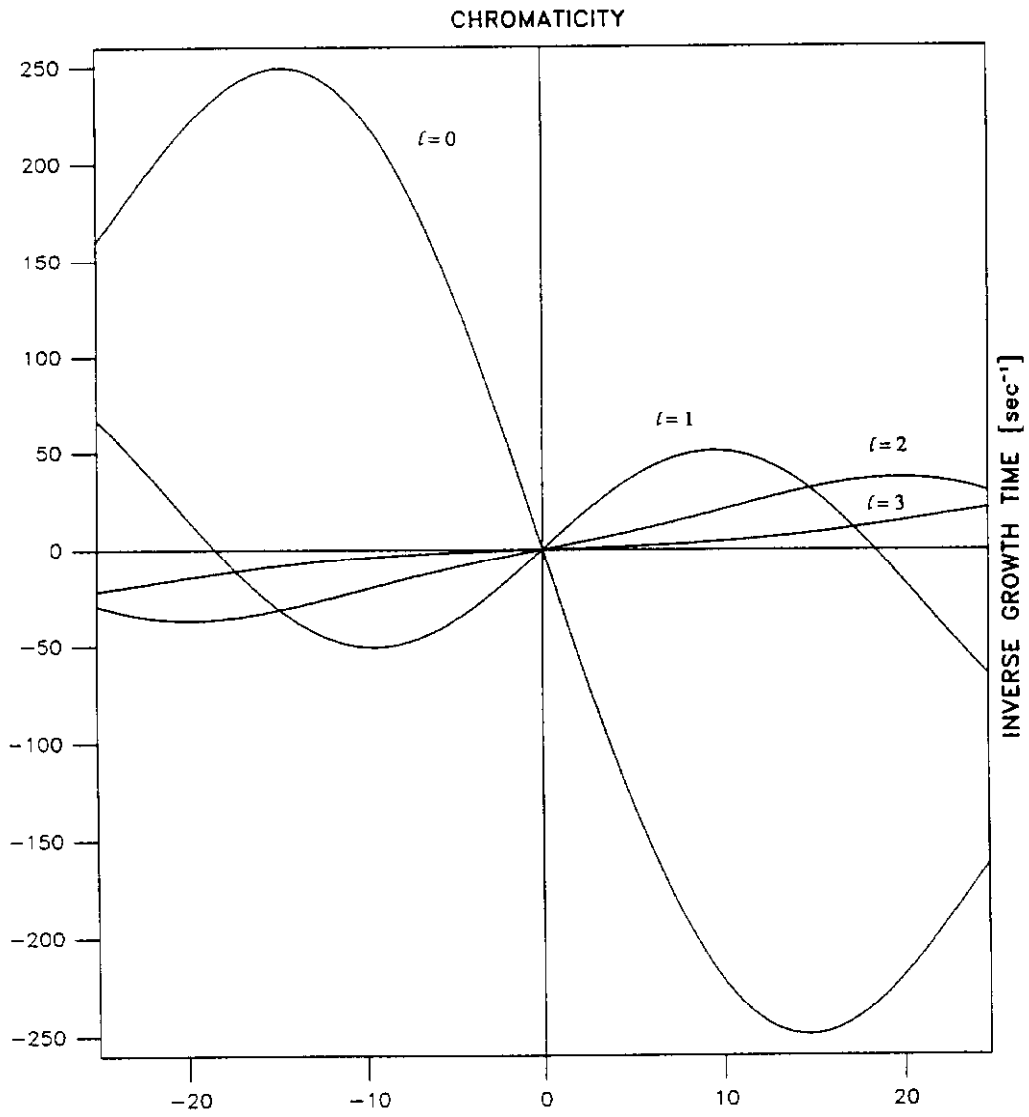


Fig. 20a

Tevatron (fixed target) p-injection @ 150 GeV

$\varepsilon = 1.5$ eV-sec.

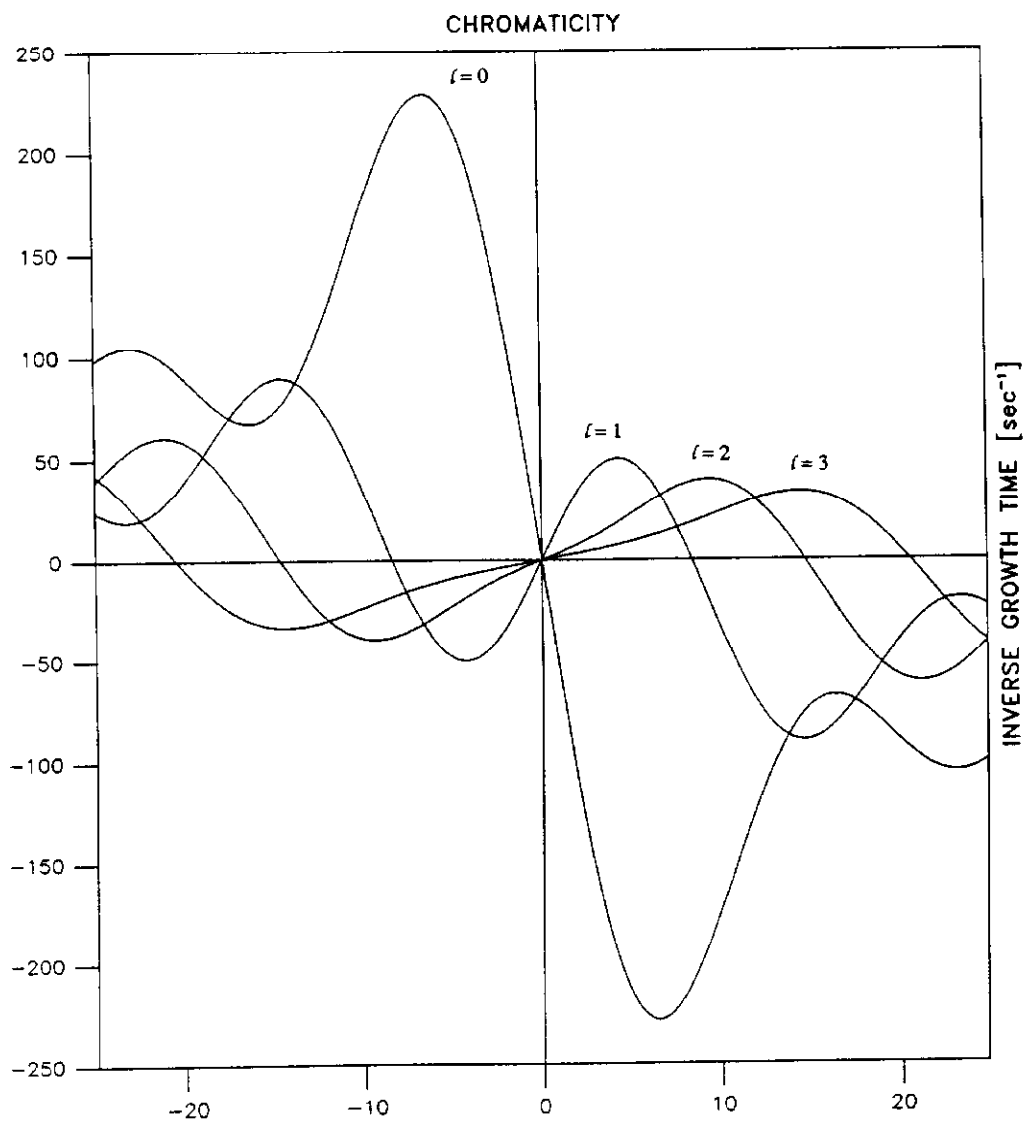


Fig. 20b

Main Ring p-injection @ 8.9 GeV

$\epsilon = 0.3$ eV-sec.

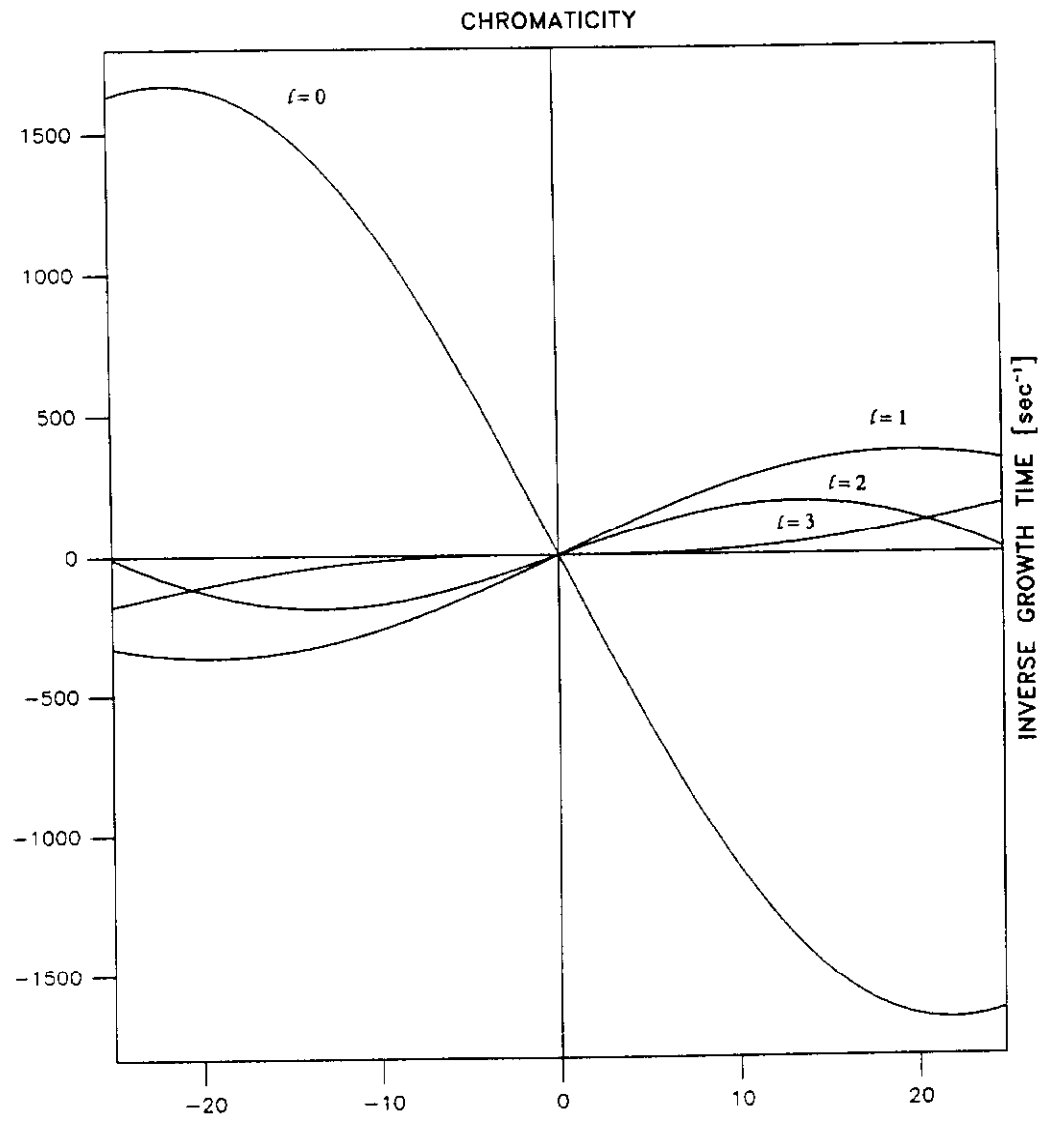


Fig. 21a

Main Ring p-injection @ 8.9 GeV

$$\varepsilon = 1.5 \text{ eV-sec.}$$

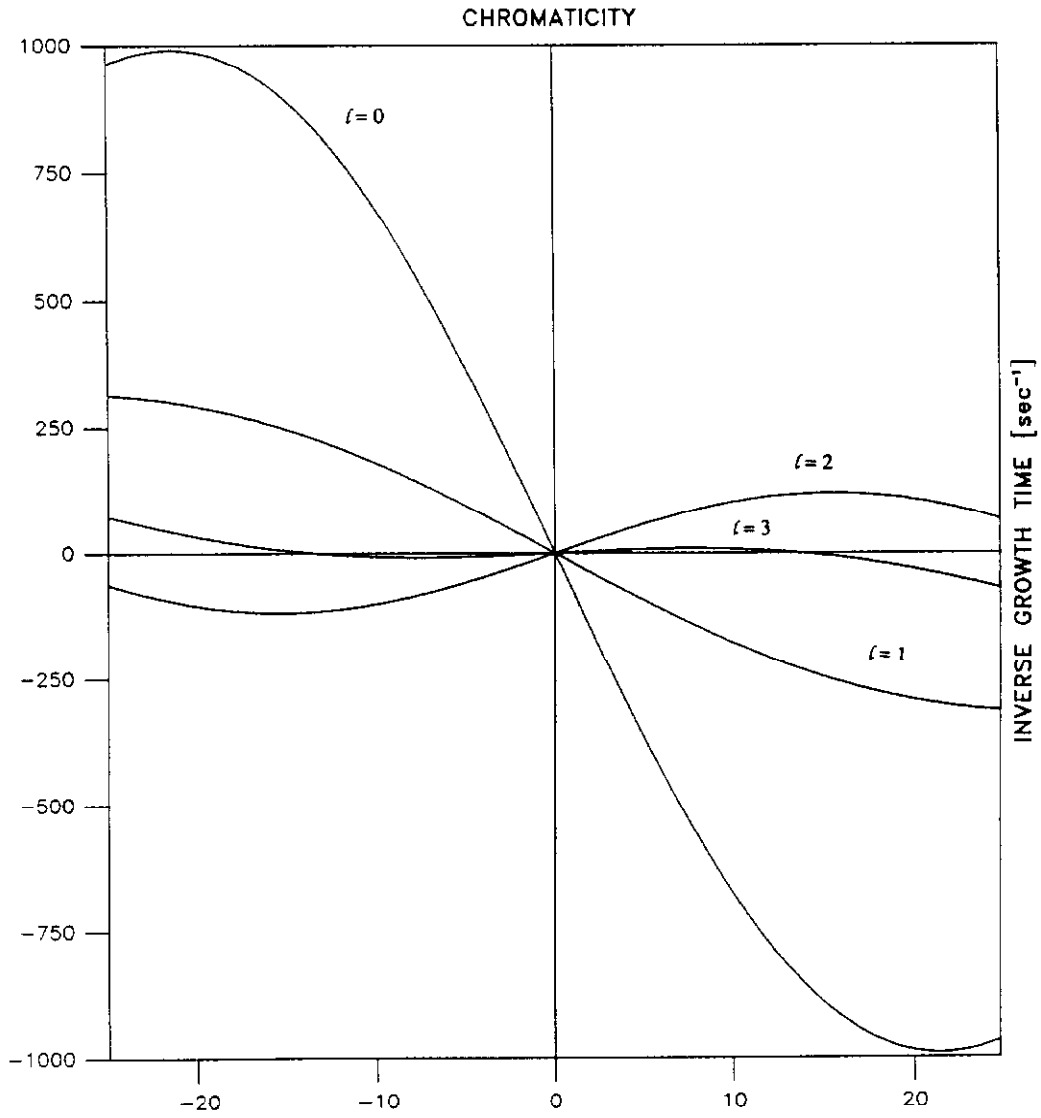


Fig. 21b

Main Injector p-injection @ 8.9 GeV

$\varepsilon = 0.3$ eV-sec.

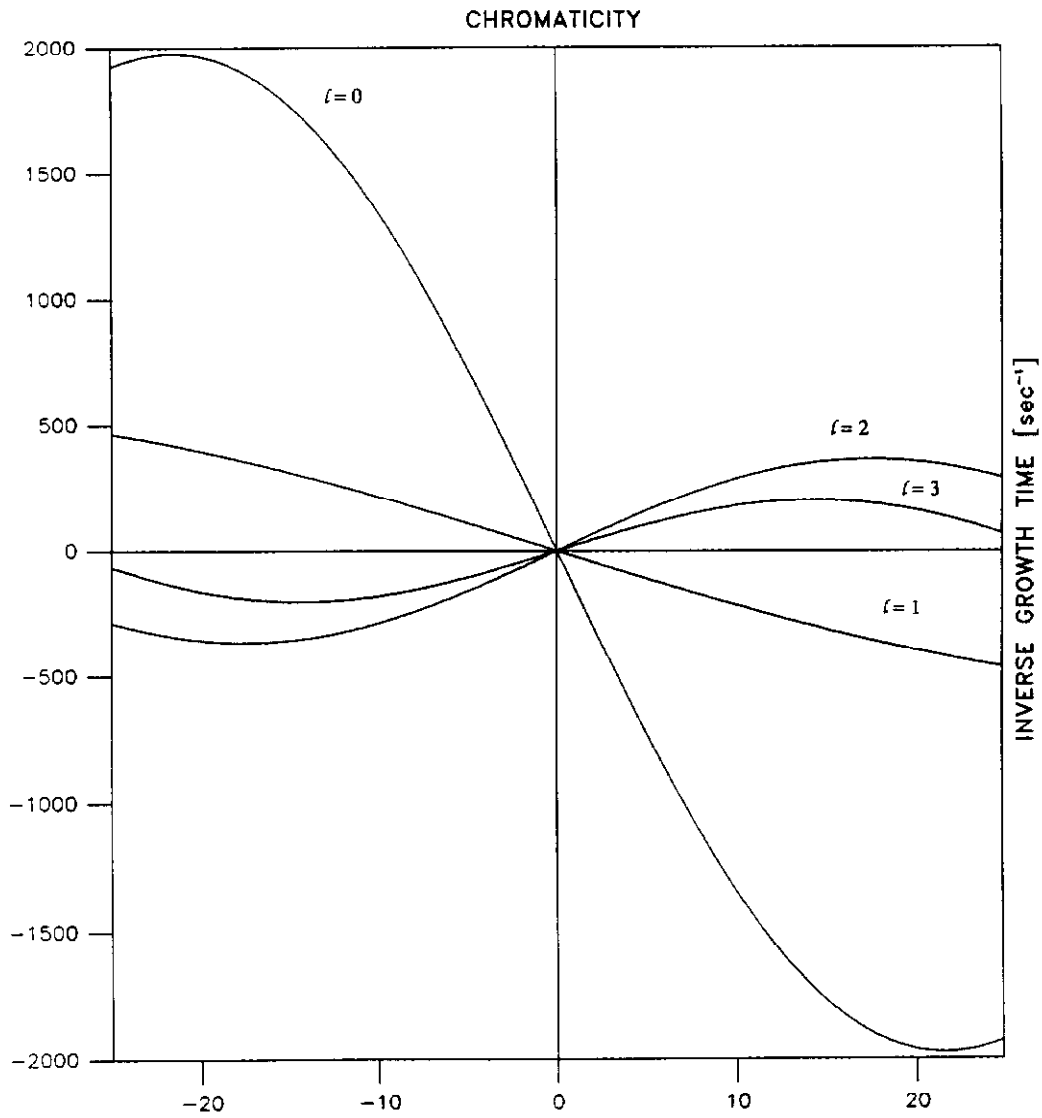


Fig. 22a

Main Injector p-injection @ 8.9 GeV

$$\varepsilon = 1.5 \text{ eV-sec.}$$

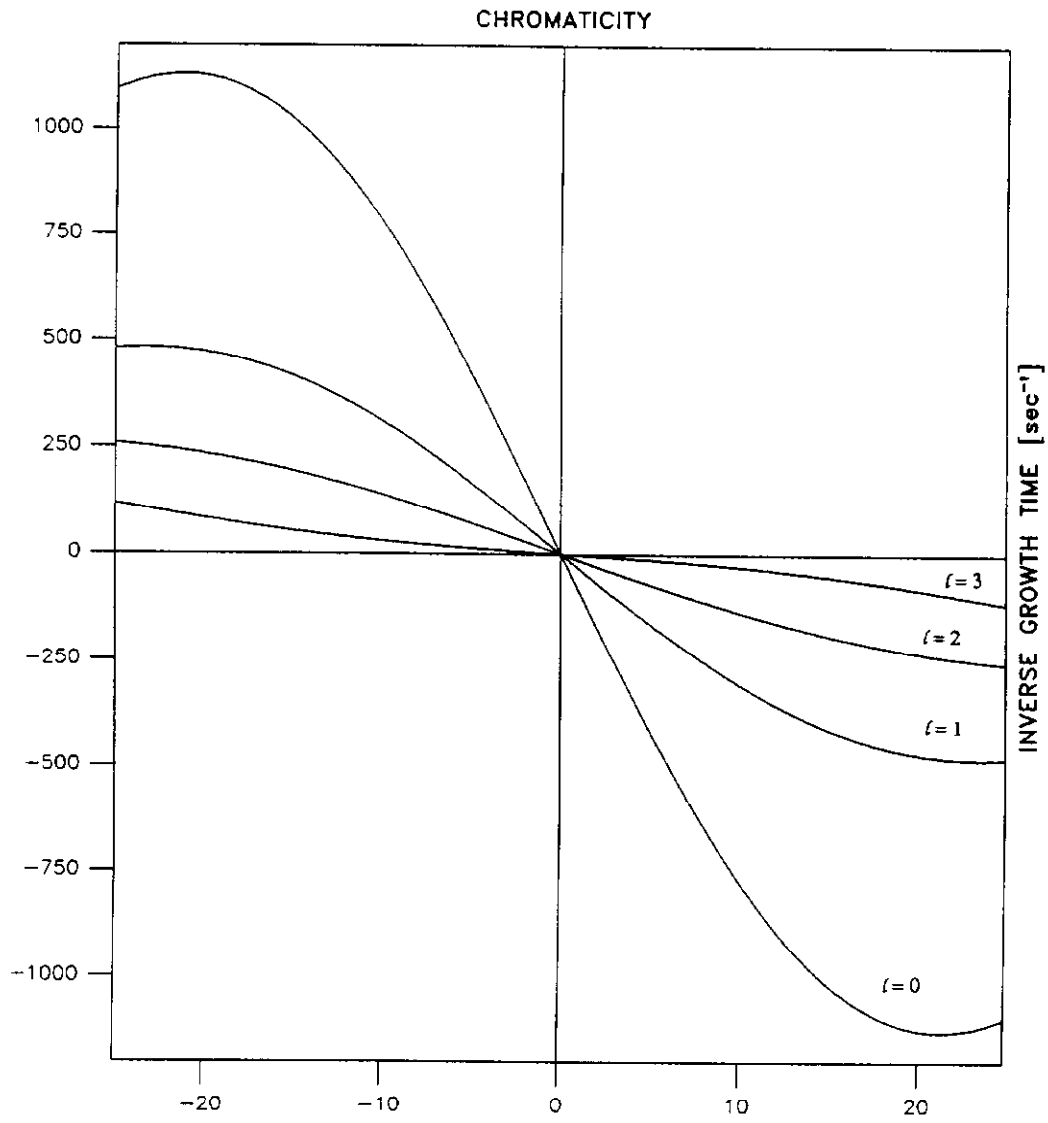


Fig. 22b